Published in final edited form as:
Prog Biophys Mol Biol. 2008 September ; 98(1): 24–37. doi:10.1016/j.pbiomolbio.2008.05.002.

Dynamics of Human Atrial Cell Models: Restitution, Memory, and Intracellular Calcium Dynamics in Single Cells

Elizabeth M. Cherry[a,b], **Harold M. Hastings**[b], and **Steven J. Evans**[c]

a*Department of Biomedical Sciences, College of Veterinary Medicine, Cornell University, Ithaca, NY 14853 USA*

b*Department of Physics and Astronomy, Hofstra University, Hempstead, NY 11549 USA*

c*The Heart Institute, Beth Israel Medical Center, New York, NY 10003 USA*

Abstract

Mathematical models of cardiac cells have become important tools for investigating the electrophysiological properties and behavior of the heart. As the number of published models increases, it becomes more difficult to choose a model appropriate for the conditions to be studied, especially when multiple models describing the species and region of the heart of interest are available. In this paper, we will review and compare two detailed ionic models of human atrial myocytes, the Nygren et al. model (NM) and the Courtemanche et al. model (CM). Although both models include the same transmembrane currents and are largely based on the same experimental data from human atrial cells, the two models exhibit vastly different properties, especially in their dynamical behavior, including restitution and memory effects. The CM produces pronounced rate adaptation of action potential duration (APD) with limited memory effects, while the NM exhibits strong rate dependence of resting membrane potential (RMP), limited APD restitution, and stronger memory, as well as delayed afterdepolarizations and auto-oscillatory behavior upon cessation of rapid pacing. Channel conductance modifications based on experimentally measured changes during atrial fibrillation modify rate adaptation and memory in both models, but do not change the primary rate-dependent properties of APD and RMP for the CM and NM, respectively. Two sets of proposed changes to the NM that yield a spike-and-dome action potential morphology qualitatively similar to the CM at slow pacing rates similarly do not change the underlying dynamics of the model. Moreover, interchanging the formulations of all transmembrane currents between the two models while leaving calcium handling and ionic concentrations intact indicates that the currents strongly influence memory and the rate adaptation of RMP, while intracellular calcium dynamics primarily determine APD rate adaptation. Our results suggest that differences in intracellular calcium handling between the two human atrial myocyte models are responsible for marked dynamical differences and may prevent reconciliation between the models by straightforward channel conductance modifications.

Keywords

human atrial cell models; restitution; memory; atrial fibrillation; delayed afterdepolarizations

Corresponding author: Elizabeth M. Cherry, Department of Biomedical Sciences, College of Veterinary Medicine, Cornell University, Ithaca, NY 14853, Phone: (607)-253-3075, Fax: (607)-253-3851, Email: emc58@cornell.edu.

1. Introduction

The development of mathematical models of cardiac cell electrophysiology has expanded greatly in recent years. The increased availability of experimental data has made increasingly specialized models possible, so that models now exist for the atria and ventricles of several species as well as for Purkinje and sinoatrial node cells. In some cases, different formulations of these models have been developed to reproduce spatial variations in electrophysiology, such as through the ventricular wall or in different locations in the atria. Furthermore, models incorporate varying degrees of complexity and may describe transmembrane currents using traditional Hodgkin-Huxley gating variables or Markov chains, intracellular calcium handling with simple empirical functions or more biophysically detailed models of buffering and sarcoplasmic reticulum uptake and release of calcium, and ion channel distribution as uniform or with spatial variations and associated gradients of ion concentrations within the cell, among others.

Modeling and simulation offer several benefits to complement traditional cell-based experiments. They allow systematic variation of parameters while retaining complete reproducibility. Experimental conditions like noise as well as statistical variability can be controlled directly. All variables and currents can be accessed, making it possible to analyze their interactions. Finally, robustly constructed models allow insights into mechanisms, which can be used to formulate new testable hypotheses and ultimately to assist in expanding the understanding of cell behavior.

Although models offer these benefits, the increased complexity of models has made an understanding of their full range of properties extremely difficult. Nonetheless, multiple models of the same species and region of the heart should predict similar properties and behavior, because they describe the same system. In this paper, we review two models of the human atrial action potential developed by Nygren et al. (1998) and by Courtemanche et al. (1998). Because they both represent human atrial cells and because they draw from largely the same experimental data, the two models would be expected to share a number of properties. Nevertheless, the models appear different even when comparing a single action potential from each at a long cycle length (CL), as the Nygren et al. model (NM) produces a triangular action potential, while the Courtemanche et al. model (CM) produces an action potential with spike-and-dome morphology. Some comparisons of the two models already have been performed by Nygren et al. (2001), who concluded that the two models were largely similar and that the differences in action potential morphology and other properties could be explained as arising primarily from differences in current magnitudes.

However, properties of these models including rate dependence, memory, alternans dynamics, and afterdepolarizations have not been analyzed in detail. In this review, we will first discuss the similarities and differences of the formulations of the NM and the CM. Then we will review the rate dependence of action potential durations (APDs) and amplitudes and resting membrane potentials (RMPs) along with the memory properties of these two models. We also will discuss how for a wide range of conditions, the NM can exhibit delayed afterdepolarizations that can become full-scale action potentials after long-term rapid pacing is stopped. Then, we will expand our discussion to include several variants of the models, in which currents are rescaled to simulate the other model and to simulate electrophysiological remodeling that arises from prolonged AF. Finally, we will review model behavior resulting from interchanging the transmembrane current formulations while retaining the original descriptions of intracellular calcium handling.

2. Model formulations

Two different models of the human atrial action potential have been developed. Each of the two models was developed using Hodgkin-Huxley-style gating variables, detailed intracellular calcium handling, and the same transmembrane currents. The Nygren et al. model (NM) (Nygren et al., 1998) uses 29 variables, 12 transmembrane currents, a two-compartment sarcoplasmic reticulum (SR) and restricted subsarcolemmal space for calcium handling, varying dyadic cleft ionic concentrations, and calcium buffering to describe human atrial myocyte electrophysiology. The Courtemanche et al. model (CM) (Courtemanche et al., 1998) has 21 variables, expressions for the same 12 transmembrane currents, and intracellular calcium handling with a two-compartment SR and buffering. The models are based largely on the same human studies for the fast Na^+ current I_{Na}, the transient outward K^+ current I_{to}, the ultrarapid delayed rectifier K^+ current I_{Kur} (referred to as I_{sus} by Nygren et al. (1998), but derived from similar data as I_{Kur} (Courtemanche et al., 1998) and referred to hereafter only as I_{Kur} for consistency), the L-type Ca^{2+} current $I_{Ca,L}$, the rapid delayed rectifier K^+ current I_{Kr}, the slow delayed rectifier K^+ current I_{Ks}, and the inward rectifier K^+ current I_{K1}, while using different previous models as the basis for the remaining currents and intracellular calcium handling (Lindblad et al. (1996) for the NM and Luo and Rudy (1994) for the CM).

The original NM also specifies the use of an electroneutral Na^+ influx term, $\Phi_{Na,en}$, which is used to achieve ionic homeostasis when paced at a frequency of 1 Hz. However, the model did not assign a charge carrier to the stimulus current, as suggested subsequently by Hund et al. (2001). The current integral of the electroneutral flux over one action potential (AP) at a cycle length (CL) of 1000ms is exactly equal to the current integral of the specified stimulus current for the same amount of time. Therefore, the electroneutral Na^+ influx term can be eliminated and instead the method of Hund et al. (2001) can be adopted by considering the stimulus current to be an additional current mediated by sodium. In this case, the stimulus current is used to update the concentrations of both $[Na^+]_i$ and $[Na^+]_c$ in place of the electroneutral Na^+ influx.

Ionic concentrations in the NM evolve in a highly nonlinear manner and do not reach steady state after several minutes of pacing at fast rates, despite treating the stimulus current as a charge carrier as described. Figure 1 shows intracellular and extracellular cleft space concentrations of Ca^{2+}, Na^+, K^+ over 10 minutes of pacing at CLs of 1000, 500, and 350 ms. For this reason, simulations an be conducted both with all concentrations allowed to vary and as a variant referred to as the NMf, in which all cleft space concentrations as well as $[Na^+]_i$ and $[K^+]_i$ are held fixed to their initial values. In the CM, the ionic concentrations $[Na^+]_i$ and $[K^+]_i$ experience drift, but at a much more gradual rate. Over 10 minutes of pacing, $[Na^+]_i$ increases by 0.76, 0.82, and 0.80 percent for CLs of 1000, 500, and 350 ms, while $[K^+]_i$ decreases by 0.11, 0.14, and 0.17 percent for the same CLs (not pictured). Because $[Na^+]_i$ and $[K^+]_i$ experience very slow linear drift that is not eliminated by assigning a charge carrier to the stimulus current following the method of Hund et al. (2001), it is common to treat these values as constant (Xie et al., 2002).

In all other respects, the basic NM and CM models for the purposes of this review are implemented as described by Nygren et al. (1998) and Courtemanche et al. (1998), respectively, with the exception of several minor corrections to the NM: the repolarizing currents I_{Kr} and I_{Ks} are included in the differential equation of the voltage, the sign of the calcium diffusion current I_{di} in the differential equation for subsarcolemmal space calcium is corrected to be positive, and the value of k_{Ca} is set to 0.025 mmol/L. The methods of Rush and Larsen (1978) and Victorri et al. (1985) were used to improve computational efficiency.

This paper also reviews a number of variants of the basic models, as listed in Table 1. Two sets of changes to transmembrane current conductances have been proposed to improve

agreement in the baseline AP morphology of the two models. Nygren et al. (2001) proposed modifying the NM to produce behavior more similar to the CM by multiplying $I_{Ca,L}$ by 1.33, I_{to} by 2, I_{Kur} by 0.4, and both I_{Kr} and I_{Ks} by 3, a model variant we refer to as the NM-C or NMf-C when concentrations are allowed to vary or are held fixed as described above, respectively. The inverse of these changes can be applied to the CM to attempt to produce more NM-like behavior, a model variant referred to as CM-N. Syed et al. (2005) proposed to change the conductances of the NM directly. These changes, which are incorporated here as specified for the four-frequency parameter fitting of Syed et al. (2005), correspond to multiplying I_{Na} by 0.938, $I_{Ca,L}$ by 1.37, I_{to} by 2.07, I_{Kur} by 0.196, I_{Ks} by 1.50, I_{Kr} by 1.56, I_{K1} by 1.07, $I_{Na,b}$ by 1.02, and $I_{Ca,b}$ by 1.02. In addition, all cleft space concentrations along with $[K^+]_i$ and $[Na^+]_i$ are held constant, as described earlier for the NMf variant. The resulting model variant is referred to as the NMf-C2.

For both models, the effects of electrophysiological remodeling by prolonged atrial fibrillation (AF) can be simulated by decreasing several currents, following Courtemanche et al. (1999), and the resulting models are referred to as CM-AF for the CM and as NM-AF or NMf-AF for the NM with varying and fixed concentrations, respectively. Specifically, for these cases, $I_{Ca,L}$ is reduced to 30 percent of its original value, and both I_{to} and I_{Kur} are reduced to 50 percent of their original values.

Additional model variants can be created by interchanging all 12 transmembrane current descriptions while retaining the original formulations for intracellular calcium dynamics, including buffering, and intracellular and all ionic concentrations. Thus, the CM-X uses the calcium handling of the CM together with the transmembrane current formulations of the NM, with the NM-X and NMf-X developed similarly. This procedure allows the relative roles of transmembrane currents and intracellular calcium to be assessed.

3. Properties of the original models

3.1 Transmembrane currents

The NM and CM include essentially the same transmembrane currents, but these currents are formulated differently. Some currents, including I_{Na}, I_{Kr}, I_{Ks}, I_{to}, I_{Kur}, I_{K1}, and $I_{Ca,L}$, are based on data from human atrial myocytes for both models (Nygren et al., 1998; Courtemanche et al., 1998), while the remaining currents are based on other models with minimal modifications to current magnitudes (Lindblad et al. (1996) for the NM and Luo and Rudy (1994) for the CM). Nygren et al. (2001) find many similarities between the major currents of the models, with differences primarily accounted for by variations in current magnitudes. However, differences can be seen in the currents as well, especially in their rate dependence. Figure 2 shows some of the major transmembrane currents functioning early in the AP for both models at CLs of 1000 ms (bold), 500 ms, and 350 ms. The CM shows adaptation to rate after the upstroke and this is reflected in the rate dependence of $I_{Ca,L}$ and I_{Kur}. In contrast, limited rate dependence is seen in the AP for the NM despite visible changes in $[Ca^{2+}]_i$, $I_{Ca,L}$, and I_{to}. Significant differences in individual currents can be seen between the models as well, with increased duration and rate dependence of $I_{Ca,L}$ and I_{Kur} along with decreased rate dependence of I_{to} in the CM compared to the NM. The calcium transient $[Ca^{2+}]_i$ is also different, with a more gradual, longer-lasting transient in the CM compared to a much sharper transient in the NM.

Different currents also participate during the remainder of the APs for the two models, as shown in Figure 3. Both $I_{Ca,L}$ and I_{Kur} are stronger over more of the plateau and repolarization AP phases in the CM than in the NM, and I_{Kr} and I_{Ks} are activated differently and have larger magnitudes in the CM as well (I_{Kr} is so small in the NM that it is only minimally involved). I_{Ks} is more important later in the CM AP at long CLs, with the maximum current occurring

during repolarization, while the magnitude of I_{Ks} is much smaller in the NM and its maximum occurs during the upstroke. I_{K1} is similar in both cases, with limited rate dependence. These currents contribute to the overall rate dependence of APD of the models, as discussed below. The NM also has a strong rate dependence of resting membrane potential (RMP), which occurs at least in part because of its smaller I_{K1} conductance.

Nygren et al. (2001) reported that most of the transmembrane current formulations of the two models were quite similar, and that the main differences between the models were the choice of baseline action potential morphology (triangular for the NM, spike-and-dome for the CM), the robustness of the resting membrane potential, and the conductances assigned to the different currents. The primary difference in action potential morphologies was used to explain several differences in model behavior, including rate dependence (which required larger $I_{Ca,L}$, I_{Kr}, and I_{Ks}, as in the CM) and the response to I_{Kur} blockade (which resulted in substantial prolongation for the triangular NM AP, which depended on I_{Kur} for repolarization, but did not prolong the spike-and-dome CM AP, which relied more on I_{Kr} and I_{Ks} for repolarization). However, despite certain similarities, differences remain among the current descriptions and their dependence on other quantities, such as ionic concentrations, as well as in the time constants of the gating variables, which can vary substantially not only in magnitude but in the voltage range where the maxima and minima are located.

3.2 Rate dependence and restitution of APD

The two models show different responses to changes in rate, most noticeably in their AP morphologies: the NM AP has a triangular shape at all cycle lengths (CLs), while the CM AP has a spike-and-dome morphology at long CLs that becomes triangular at shorter CLs. Figure 4A–C illustrates the APs of the CM and NM with both fixed (NM) and varying (NM-f) concentrations after pacing for 30 seconds at CLs of 1000ms, 500ms, and 350ms. The CM, as expected, exhibits spike-and-dome morphology at 1000ms, with the dome evolving to a relatively flat plateau at 500ms and disappearing by 350ms. The NM remains triangular over all CLs. The two models also exhibit different resting membrane potentials (RMPs). For the CM, the RMP is −81 mV at 1000ms and the increase with pacing rate is only slight. The NM has a higher RMP of −74mV, and this RMP is more sensitive to rate, especially with fixed concentrations. As a result of both increased RMP and decreased upstroke peak potential, action potential amplitude (APA) overall decreases with rate in both models (see Fig. 4D), but more strongly for the NM than for the CM: APs at a CL of 350 ms retain 94% of their amplitude at a CL of 1000 ms for the CM, but decrease to 89% and 80% for the NM with varying and fixed concentrations, respectively, owing to both increased RMP and decreased maximum upstroke voltage.

Rate dependence can be assessed by steady-state restitution curves (also known as dynamic restitution curves (Koller et al., 1999)), which are obtained by pacing at each of a range of CLs for a fixed amount of time (30 seconds in this review, except where noted otherwise) and recording the last APD and the preceding diastolic interval (DI) (or the last two APDs and their preceding DIs when alternans are present). Measuring APD restitution in a useful manner for these models requires using a CL-dependent threshold for determining APD. When the same voltage threshold is used for all CLs in a steady-state restitution protocol, differences in RMP and APA, which can become quite substantial at short CLs (see Fig. 4D), are ignored. This can lead to two effects that do not represent the model's dynamics appropriately, as demonstrated in Figure 5A–C, where APD is calculated as a function of DI using either a CL-dependent threshold for APD_{90} (solid) or a fixed threshold corresponding to APD_{90} at a CL of 1000 ms (dashed). First, the restitution curve using a fixed voltage threshold overall is shifted toward smaller DIs, as shown for all three models in the dashed line curves. This effect occurs because the RMP at fast rates eventually becomes higher than the fixed voltage threshold corresponding

to APD_{90} at 1000ms, even though the cell is still excitable, so that the minimum DI is incorrectly measured in all three models as 0 (or negative DIs can be computed, although this requires extrapolation of the action potential that must be based on unverifiable assumptions). Second, the APDs measured at small DIs are overstated when the fixed threshold is used. This occurs because the increasing RMP at short CLs becomes very close to the fixed voltage threshold, so that the voltage threshold more closely corresponds to higher repolarization values than 90 percent, an effect that can lead to flatter or even supernormal restitution curves. For the CM (Fig. 5A), the curves measured using the different measurements of APD do not differ much until DIs below 100 ms. However, for the NM (Fig. 5B), the overall shape of the curve changes and shows supernormality with a non-varying threshold, whereas with CL-dependent thresholds, the curve has no supernormality. The NMf (Fig. 5C), which exhibits the largest sensitivity of RMP to CL, shows the greatest increase in APD at short DIs with a non-varying threshold, leading to a supernormal restitution curve over all CLs, whereas supernormality is only slight in magnitude and is present only for DIs larger than 250 ms when a CL-dependent threshold is used. It is also possible to reduce the effect of threshold choice by constructing restitution curves using refractory periods instead of APDs (Xie et al., 2002); however, many additional stimuli are required to find the refractory period, and the DI still must be determined, so that in this review we concentrate on standard APD restitution curves.

Steady-state APD restitution curves are generated by taking the last DI and APD measured after 30 seconds of pacing at each CL of interest, and indeed, by 30 seconds, both the CM and NMf reach a steady-state. However, the NM continues to experience changes in ionic concentrations that lead to continuing variation in APD, even when measured after pacing for up to several minutes. Figure 5D and E show differences in steady-state restitution curves obtained for the NM and NMf after pacing at each CL for 5, 10, 30, and 60 seconds. Although the NMf (Fig. 5E) reaches a steady state after 30 seconds of pacing, such that additional pacing at the same CL does not result in further changes in APD, the NM (Fig. 5D) exhibits continual decreases in APD depending on the duration of pacing over almost the full range of DIs. To minimize the effects of continual concentration drift over time that can build up over multiple CLs, initial conditions are reset to those for a CL of 1 s as specified by Nygren et al. (1998) after each CL in the restitution protocol for the NM. Because of the adaptability of the model to CL changes, the reset initial conditions do not lead to 2:1 block at any CL.

Steady-state APD restitution curves obtained by using a CL-dependent threshold for APD_{90} over all CLs and a fixed stimulation time of 30 s are shown in Figure 4E–G. In general, these restitution curves, shown as solid lines, are relatively flat for both models. At the shortest DIs, the slope steepens significantly as the APD decreases rapidly. In the NM in particular, very small APDs can be achieved because of dramatic decreases in APA while the cell is still responsive to stimulation; however, all three models show responses at very short CLs. These responses do show a small amount of I_{Na} activation and nonlinear inactivation, and therefore they appear to be true APs, rather than simply a return to RMP following injection of a stimulus current. However, these short APs do not propagate in 1d and therefore are not relevant in tissue, and use of a threshold of I_{Na} magnitude in determining whether a response is an AP or not could modify the minimum DI and CL in an isolated cell.

Overall, the two models show different responses to changes in rate. The primary differences are increased APD for the CM compared to the NM and NMf and substantially increased RMP as the CL is decreased for the NM and NMf compared to a more modest increase for the CM. The increase in RMP with decreased CL is consistent with observations in isolated human atrial myocytes, where RMP has been measured to increase 19 mV from pacing at 800 ms to pacing at 100 ms (Workman et al., 2001). APDs for all models are longer than those reported for isolated human atrial myocytes by Workman et al. (2001) (210 ms at a CL of 800 ms down to 75 ms at a CL of 100 ms), with the NM closest. Restitution curve slopes greater than one

appear only for very short DIs, below 43, 42, and 71 ms for the CM, NM, and NMf, respectively. A slight degree of alternans at a CL of 100 ms and 4:4 dynamics at 95 ms (shown as filled circles), with a return to 1:1 behavior at 90 ms, occurred for the CM. Alternans did not occur for the NM or for any AF variation of either model. This suggests the possibility that atrial arrhythmias may rely more heavily on other AF-induced changes, including not only electrophysiological differences but also structural features, such as atrial enlargement, increased fibrosis, and spatial heterogeneity (Li et al., 1999; Schotten et al., 2003).

3.3 Short-term memory properties

Both models possess short-term memory, which reflects the fact that APD is not well-predicted simply by the previous DI alone but includes a "memory" of previous activations. The memory properties of the models can be measured by using a different restitution protocol, the S1S2 protocol, rather than the steady-state protocol already used. In the S1S2 protocol, S1S2 restitution curves are computed by pacing for a given time (in this review, 30 s) at a fixed CL (termed S1, or stimulus 1) and then introducing a single subsequent stimulus over a range of intervals (S2); the APD following each S2 stimulus and the preceding DI are recorded to generate a curve that in general is dependent on S1. The S1S2 protocol therefore produces a family of curves for different values of S1 and can be used to quantify memory (Cherry and Fenton, 2007). For the S1S2 restitution curves, the threshold is set to the voltage value that defines 90 percent of repolarization for the S1 CL.

S1–S2 restitution curves obtained for the models with different S1 CLs are shown in Figure 4E–G. The NM with varying concentrations consistently displays the greatest variation in APD for a given premature S2 stimulus as a function of the S1 CL; however, the NMf and CM also show S1-dependent changes. In all cases, the S1–S2 curves are fairly shallow, and in general were less steep than the steady-state restitution curves. For the NM, APDs decrease with decreasing S1 CL. This is also the case for the CM at long DIs, but for short DIs below about 200 ms, the reverse is true. For the NMf variant, the dynamics are more complex, with APDs over all DIs first increasing with a decrease in S1 CL and then decreasing with further S1 decreases. APD prolongation with decreasing S1 CL is correlated with biphasic restitution curves, which can be seen for the NMf in Figure 4G and which occurs only at longer DIs for the CM (>600 ms) than can be seen in Fig. 4E. The maximum DI that can be used slightly decreases as the S1 CL decreases. Note that long DIs often cannot be used in S1–S2 protocols for the NM and NMf because of the occurrence of delayed afterdepolarizations before the S2 can be applied (see below).

3.4 Delayed Afterdepolarizations

Following cessation of pacing, the NM but not the CM can exhibit auto-oscillatory behavior under a wide range of conditions due to delayed afterdepolarizations (DADs). In general, fast rates prior to pacing cessation are needed to produce DADs, which can be manifest as a small number of beats or as a prolonged series of beats that can last 30 seconds or longer. The frequency of these series of oscillations tends to decrease over time. The DADs may produce small-amplitude oscillations or full-amplitude APs. While many factors can enhance or suppress the DADs, the underlying substrate that allows DADs to develop stems from intracellular calcium dynamics. Intracellular calcium handling in the NM is complex, including four calcium concentration variables representing the intracellular medium, the restricted subsarcolemmal space, and the SR uptake and release compartments, as well as five variables that represent calcium buffering processes by tracking the fractional occupancy of calmodulin and troponin buffers in the cytoplasm and calsequestrin in the SR. The intricate interactions among the intracellular calcium variables can allow DADs to be produced, and changes that affect intracellular calcium can facilitate or hinder the generation of such DADs. Fundamentally, however, the DADs are produced when intracellular calcium increases during

diastole and results in calcium release from the SR, and the increased inward sodium-calcium exchange current I_{NaCa}, working to extrude calcium, causes an increase in membrane potential.

Figure 6 shows DADs induced or prevented under a wide range of conditions. In all cases, periodic pacing is applied to the cell for 30 seconds, after which time (t=0 ms) the cell is observed for another 30 seconds. In Fig. 6A, DADs are produced after ceasing pacing at a period of 350 ms (dotted). These DADs are spaced farther and farther apart until they die out completely after about 17 s. Afterdepolarization activity is enhanced by following the same procedure with the buffering variable O_{TMgMg} (which tracks the fractional occupancy of the troponin-Mg^{2+} buffer by Mg^{2+}) held constant at its initial value throughout the simulation (solid). In this case, the DADs occur repetitively during the entire 30 second observation period, although slowing is observed over time.

Pacing rate before cessation of pacing also affects the inducibility of DADs. In Fig. 6B, three pacing CLs of 1050 ms (solid), 700 ms (dotted), and 350 ms (dashed) are used. For the longest CL of 1050 ms, no DADs develop. After the 700 ms rate, a series of DADs develop at a slow rate, with about 2 s passing between the first two afterdepolarizations. Following the 350 ms rate, two low-amplitude DADs develop in rapid succession without developing into full-amplitude APs, but the third and later DADs result in full APs initially spaced less than 1 s apart.

For a fixed rate, various modifications can affect the development of DADs. As shown in Fig. 6C, holding O_{TMgMg} constant (dotted) enhances DADs and increases their frequency compared with the control case at the same CL of 350 ms (dashed), while holding the buffering variable O_{TC} (fractional occupancy of the troponin-Ca^{2+} buffer by Ca^{2+}) constant (solid) prevents the development of DADs. It is also possible to suppress DADs by increasing the time rate of change of the buffer occupancy, dO/dt, by a factor of 4 (Fig. 6D, dotted) or by decreasing the magnitude of the Na^{+}-Ca^{2+} exchange current I_{NaCa} to 10 percent of its original value (solid). Substantial alterations to the magnitudes of other transmembrane currents can prevent DADs as well, such as increasing I_{Kr} by a factor of 500 (Fig. 6E, dotted) or increasing I_{K1} by a factor of 10 (Fig. 6E, solid).

Because the DADs develop more slowly than regular APs, it is possible to observe the initial depolarization of membrane potential but to stimulate the cell before the DAD would have occurred, especially for some parameter regimes. The appearance of DADs also can reduce the range of S1S2 restitution curves that can be obtained, by preventing the use of short S1 CLs, long S2 coupling intervals, or both, as can be seen for certain variations of the NM.

DADs develop in the NM when the delicate balance of factors affecting $[Ca^{2+}]_i$ during recovery after an AP shifts so that $[Ca^{2+}]_i$ begins to increase. Once the balance tips in favor of $[Ca^{2+}]_i$ increase, the SR releases Ca^{2+} and I_{NaCa} increases in magnitude to extrude Ca^{2+}. As intracellular Ca^{2+} continues to rise, I_{NaCa} continues to increase, thereby producing a DAD that increases the membrane potential. If the change in potential is large enough, the cell can depolarize above threshold, at which point I_{Na} activates and an AP is generated. This can be seen in Fig. 7, which depicts the last of a train of paced APs at a CL of 350 ms followed by cessation of pacing at time t=0 ms. The solid trace shows DADs that occur when O_{TMgMg} is held constant while the dashed trace shows the absence of DADs when O_{TC} is held constant. Note that the DAD-induced AP (Fig. 7A) has a much broader foot and slightly decreased phase 0 amplitude compared with the paced AP. When O_{TMgMg} is held constant, I_{NaCa} magnitude increases (Fig. 7B) in response to Ca^{2+} release (Fig. 7C) and increased intracellular Ca^{2+} (Fig. 7D) and produces the series of DADs. Because the depolarization by I_{NaCa} is gradual until the higher voltage triggers the activation of I_{Na}, the early upstroke of the DAD-induced AP is quite broad.

The balance of transmembrane and intracellular Ca^{2+} currents that define the time rate of change of $[Ca^{2+}]_i$ are shown in Fig. 7E. Before the normal beat, this derivative remains negative or zero, which prevents Ca^{2+} from increasing. When pacing is stopped, however, the derivative changes sign, leading to an increase in $[Ca^{2+}]_i$. Because the sign of the derivative depends directly on the balance of three transmembrane currents (I_{NaCa}, the background calcium current I_{Cab}, and the sarcolemmal pump current I_{pCa}), three intracellular calcium currents (the restricted subsarcolemmal space to cytosol diffusion current I_{di}, the SR uptake current I_{up}, and the SR release current I_{rel}), and the rate of change of three calcium buffering variables (O_{TC}, the fractional occupancy of the troponin-Mg^{2+} buffer by Ca^{2+} O_{TMgC}, and the fractional occupancy of the calmodulin buffer by Ca^{2+} O_C), and because these variables in turn depend on each other and other variables in a highly nonlinear way, a broad range of interventions can facilitate or prevent DADs following cessation of pacing.

DADs have not generally been implicated as a precursor to atrial arrhythmias. However, the DADs that occur in the NM in various parameter regimes and ventricular DADs, which can be proarrhythmic, appear to arise from similar mechanisms (Bers, 2002). The DADs in both cases arise after repolarization has largely finished and are associated with intracellular Ca^{2+} overload and release, with I_{NaCa} serving as a transient inward current that depolarizes the cell. For the NM, DADs occur more frequently at faster rates, and different parameter changes that affect the balance of calcium-related currents and fluxes can enhance or suppress DAD formation. DADs were not observed to occur in the CM for any parameter set.

4. Properties of model variants

4.1 Conductance changes to simulate other models

Two authors have proposed changes in current magnitudes of the NM to reproduce AP morphologies and other properties that more closely match the CM. Nygren et al. (2001) modify the magnitudes of $I_{Ca,L}$, I_{to}, I_{Kur}, I_{Kr}, and I_{Ks} as indicated above and in Table 1. These changes were shown previously to produce an AP whose morphology became spike-and-dome for long CLs, resembling the morphology of the CM at long CLs. To the extent that the proposed changes alter NM APs to more closely resemble those of the CM, the inverse changes would be expected to alter CM APs to more closely resemble those of the NM.

Rate dependence and memory effects can be seen in Figure 8A–C, which shows APs obtained at three different CLs using the CM-N, the NM-C, and the NMf-C. The CM-N AP (Fig. 8A), compared to the original CM, has lost its spike-and-dome morphology at a CL of 1000 ms and looks more like an AP of the NM, although it retains a longer APD and a lower and less variable RMP than the NM. These differences remain at shorter CLs. Both the NM-C (Fig. 8B) and NMf-C (Fig. 8C) have a spike-and-dome morphology at a CL of 1000 ms similar to that of the CM, although the CM AP still has a longer duration and a lower RMP. At shorter CLs, the NM-C and NM-fC remain more triangular in shape than the CM and experience greater increases in RMP.

Figure 8E–G shows the APD restitution curves for the CM-N, NM-C, and NMf-C under both steady-state and S1–S2 protocols. When compared with the restitution curves shown in Fig. 4E–G, both similarities and differences can be seen between the CM-N and the NM/NMf it seeks to imitate and between the NM-C/NMf-C and the CM they seek to imitate (shown in gray). APDs for the NM-C and NMf-C do not prolong to match the CM. Instead, the steady-state NM-C and NMf-C APDs for all CLs remain well below 220 ms, which is the minimum APD for DIs greater than 50 ms for the CM. At short DIs, the NM-C and NMf-C also more closely resemble the NM and NMf than the CM.

Memory properties also are affected by the conductance changes. The CM-N reverses the direction of its S1–S2 restitution dependence on S1 CL at short DIs: whereas the APDs prolong in the CM with decreasing S1 CL, in the CM-N APDs shorten with decreasing S1CL by about the same magnitude. However, APDs of the CM-N over most CLs are closer to those of the CM rather than to the NM or NMf. At short CLs, the CM-N develops dual APD values at short CLs. The dual values occur simply as the steady-state pacing protocol samples different short CLs and most likely are due to the differences in RMP and APA that affect the 90 percent repolarization threshold used for measuring APD. Overall, the changes that constitute the NM-C and NMf-C do not fundamentally affect the dynamics and primarily serve to introduce a spike-and-dome morphology at long CLs and to reduce APDs at shorter CLs relative to those at longer CLs by a larger degree.

The changes proposed by Syed et al. (2005) and incorporated into the NMf-C2 are based on reproducing AP morphologies and APDs (using a threshold of −60mV) of the CM after pacing for ten beats at each of four CLs (1000 ms, 500 ms, 333 ms, and 250 ms). Syed et al. (2005) find better agreement between the CM and modified NM using the parameter values proposed there than using the parameter values presented by Nygren et al. (2001). However, differences in RMP, APA and APD remain. Furthermore, the NMf-C2 is particularly susceptible to series of DADs following cessation of pacing due to gradual diastolic depolarization, which can be observed before and after the paced APs in Fig. 8D. These DADs make measuring S1–S2 restitution curves over a wide range of S2 values impossible, and for this reason they are not shown. Figure 8H shows the steady-state restitution curves for both the CM (gray) and the NMF-C2 (black), with differences in morphology (biphasic nature for the NMF-C2 but not for the CM) as well as reduced APDs for the full range of DIs and an increased DI_{min} for the NMf-C2.

Different current magnitudes can further modify restitution and memory properties. For instance, the steady-state restitution curve of the NMf can be steepened, as shown in Fig. 9A. To do so, it is important to increase the contributions of $I_{Ca,L}$ and I_{Ks} (multiplied by 1.6 and 4, respectively), which are strongly rate-dependent, and to decrease the contribution of I_{Kur} (multiplied by 0.01), which displays minimal rate dependence despite having a large magnitude (see Fig. 3). To ensure that APDs are of similar magnitude compared to those of the base model, I_{to}, I_{K1}, and I_{NaCa} are multiplied by 0.5, 0.5, and 0.1, respectively. These modifications increase the range of APDs to 62 ms over the range of DIs between 100 and 700 ms, compared to only 19 ms for the NMf, and bring the range more in line with the 46 ms range exhibited by the CM. In addition, the biphasic component of the NMf restitution curve is abolished, and the APD at a long DI of 700 ms is 276 ms, nearly as long as the 285 ms APD of the CM for the DI and much longer than the NMf's 224 ms. Note that these modifications are not intended to reproduce specific dynamics but rather are designed to serve as starting points for further investigations into the mechanisms responsible for rate adaptation and restitution in these models.

4.2 Atrial fibrillation-induced changes in rate dependence and morphology

Following Courtemanche et al. (1999), several currents can be decreased to simulate electrophysiological changes that take place as a result of sustained atrial fibrillation (AF). In this scenario, $I_{Ca,L}$ is decreased to 30 percent of its original value, and I_{to} and I_{Kur} are both decreased to 50 percent of their original values. Under these conditions, APs are triangular in morphology at all CLs and are shorter in duration. In addition, rate adaptation is largely abolished. Figure 10A–C shows APs at CLs of 1000 ms, 500 ms, and 350 ms for the CM, NM, and NMf. Other than a slight increase in RMP as the CL decreases for the NM and NMf, there is little difference from one CL to the next or even from one model to the next. Reduced rate adaptation is present for all but the very shortest CLs, as shown in Fig. 10D–F, and results in

a modest reduction in memory as well: the S1–S2 restitution curves for different S1 CLs are spaced slightly more closely together for the NM-AF and are nearly identical for the CM-AF and for the NMf-AF.

The reduction in rate adaptation shown by the models is in agreement with a number of experimental studies that show little rate adaptation in MAP recordings shortly after cardioversion of chronic AF (Franz et al., 1997; Kamalvand et al., 1999; Manios et al, 2000; Osaka et al., 2000) and in isolated myocytes (Bosch et al., 1999; Van Wagoner et al., 1999; Workman et al., 2001) and tissues (Boutjdir et al., 1986) obtained from right atrial appendage tissue of patients with chronic AF. In some cases, more significant rate adaptation can be observed at the shortest CLs (Kim et al., 2002; Dobrev and Ravens, 2003). Similar alterations to those given by Courtemanche et al. (1999) have been observed in other experiments as well (Dobrev and Ravens, 2003), including substantial reductions in $I_{Ca,L}$ (Bosch et al., 1999; Van Wagoner et al., 1999; Skasa et al., 2001; Workman et al., 2001) and I_{to} (Van Wagoner et al., 1997; Bosch et al., 1999; Brandt et al., 2000; Grammer et al., 2000; Workman et al., 2001). The reduction in I_{Kur} proposed by Courtemanche et al. (1999) has been found in some studies (Van Wagoner et al., 1997; Brandt et al., 2000) but not in others (Grammer et al., 2000; Workman et al., 2001). Additional current changes that may be important in AF-induced electrophysiological remodeling include increased I_{K1} and possible changes in the ACh-activated inward rectifier $I_{K,ACh}$ (Dobrev and Ravens, 2003). The rate dependence of RMP also was reduced in AF, with an increase of only 6 mV between CLs of approximately 800 to 120 ms (Workman et al., 2001). The models show a similar reduction in RMP rate dependence with AF-induced electrophysiological changes, especially for the NM and NMf.

In addition, the AF modifications decrease APD in all the models and also reduce memory. Separately reducing either I_{Kur} or $I_{Ca,L}$ to the level of the AF modification while keeping the other current magnitudes unchanged produces decreased memory for long CLs of the same order as for the CM-AF. However, only the reduction in $I_{Ca,L}$ results in decreasing S1–S2 restitution curves as the S1 CL decreases, as shown for the CM-AF. Thus, the decrease in memory at very short CLs for the CM-AF may be explained by the interaction between reducing I_{Ca}, and reducing I_{Kur}. The two effects combine to produce an even smaller amount of memory at short CLs. These results suggest that $I_{Ca,L}$ is responsible for the behavior of the original CM, where S1–S2 restitution curves increase as the S1 CL decreases. However, it is nonetheless possible to reverse the CM memory properties so that decreasing the S1 CL leads to decreasing S1–S2 restitution curves over all DIs even when $I_{Ca,L}$ is increased. Figure 9B shows S1–S2 restitution curves that decrease as the S1 CL decreases with the magnitudes of $I_{Ca,L}$, I_{Kur}, I_{to}, I_{Kr}, and I_{K1} multiplied by 1.5, 4, 0.1, 0.1, and 3, respectively. These interventions eliminate the biphasic morphology of the steady-state restitution curve at long DIs and produce S1–S2 restitution curves that decrease as the S1 CL is decrease. Thus, the memory effects appear to arise from complex interactions among the currents.

4.3 Interchanging transmembrane current formulations

The proposed changes to current magnitudes to increase agreement between the models still leave many differences in place. While it is possible that other choices for the model conductance values will result in improved agreement, it is also possible that the transmembrane currents play only a partial role in determining the dynamics of the models. Instead, intracellular calcium handling may contribute significantly. Because the two models contain essentially the same 12 transmembrane currents, it is possible to exchange the current formulations used to study the relative roles of the transmembrane currents in comparison to intracellular calcium handling and ionic concentrations. In this case, $[K^+]_c$ is used for $[K^+]_o$ and $[Na^+]_c$ for $[Na^+]_o$ for the CM formulation of I_{NaK} incorporated into the NM and NMf; similarly, the restricted subsarcolemmal space Ca^{2+} concentration $[Ca^{2+}]_d$ is used instead of

$[Ca^{2+}]_i$ for the CM formulation of $I_{Ca,L}$. For the NM formulation of Ca^{2+}-dependent $I_{Ca,L}$ inactivation f_{Ca} incorporated into the CM, $[Ca^{2+}]_i$ is used, and $[K^+]_o$ is used for $[K^+]_c$ in the formulation of I_{K1}.

The results of interchanging current formulations are shown in Fig. 11. Utilizing the NM current formulations increases the rate dependence of RMP in the CM-X in a manner similar to that of the original NM, while using the CM current formulations decreases RMP rate dependence for the NM-X and NMf-X. These findings strongly suggest that the transmembrane currents are largely responsible for rate differences in RMP. In contrast, the rate dependence of AP morphology and APD remain much stronger for the CM-X than for the NM-X and NMf-X. For these properties, intracellular calcium handling appears to play a more important role than the current formulations.

Memory, as evidenced by differences in S1–S2 restitution curves obtained using different values of the S1 CL, appears to be tied more closely to the transmembrane current formulations for these models. Fig. 11D shows that S1–S2 restitution curves for the CM-X first increase and then decrease with decreasing S1 CL, similar to what was seen for the NMf (Fig. 4G). The S1–S2 restitution curves for the NM-X and NMf-X (Fig. 11E–F) are clustered together more closely, with APD increasing as the S1 CL is decreased at short DIs and decreasing at long DIs. Similar behavior is observed for the CM model (see Fig. 4E).

The APDs obtained for the CM-X are longer than for the CM, and the APDs obtained for the NM-X and NMf-X are shorter than for the NM and NMf. This is not unexpected because the underlying calcium dynamics produce a longer-lasting transient for the CM than for the NM, so that the shorter CM transmembrane currents are designed to counterbalance a longer-lasting $I_{Ca,L}$ by repolarizing more quickly. When placed into the NM-X and NMf-X, then, the stronger repolarizing currents in combination with a shorter calcium transient result in shorter APDs. The opposite is also true: the NM transmembrane currents repolarize more slowly because the calcium transient is shorter, and in the setting of the CM-X produce longer APDs.

5. Implications

5.1 Agreement between the two models

The NM and CM show a number of differences in rate adaptation, restitution, and memory. Specific differences in the properties of transmembrane currents, such as their steady-state values and response to blockade, have been detailed previously (Nygren et al., 2001). Differences in the dynamics of two-dimensional reentrant spiral waves also have been shown (Nygren et al., 2001; Cherry and Fenton, 2007), with the NM showing a stable reentrant wave with a circular core and the CM showing a meandering spiral wave with mostly transient breakup. Despite these differences, it is possible that the models should not agree but instead reflect fundamental heterogeneity of human atrial myocytes. The different properties of the models may reflect actual differences in the characteristics of different regions of the atria. For instance, significant variability in AP morphology has been shown in canine atria, including differences between left and right, epicardium and endocardium, and regional structures like the crista terminalis and the appendages (Feng et al., 1998; Ramirez et al., 2000). Such variability may even exist among nearby cells and regions (Schram et al., 2002). It is also possible that AP properties may depend on other factors, including age (Jeck and Boyden, 1992) and gender (Tanabe et al., 1999; Xiao L et al., 2006).

Compared to Nygren et al. (2001), the results presented here show only slight similarities between the CM and the NMf-C or NMf-C. However, Nygren et al. (2001) compared APs only at a CL of 1000 ms, not over a broad range of CLs as done here, and even there the RMP was shown to be lower and the APD longer for the CM. Syed et al. (2005), on the other hand,

compared the CM and the NMf-C2 over a range of CLs and found good agreement. The differences between our findings using the NMf-C2 and the results presented by Syed et al. (2005) have several possible explanations. First, in Syed et al. (2005), the membrane potential data from the CM used for parameter fitting was shifted by +7mV, thereby ensuring better agreement in RMP, as this shift is equal to the difference in the RMPs of the CM and NM/NMf at a CL of 1000 ms. Second, APDs were measured by Syed et al. (2005) as the amount of time between the maximum upstroke velocity and the time at which the cell repolarized to a fixed voltage threshold of −60 mV, whereas we used a rate-dependent voltage threshold. As the RMP of the NMf-C2 increased at fast rates, −60 mV corresponded to an increasingly large percentage of repolarization compared to the same threshold for the CM, and in fact the voltage threshold representing 90 percent of repolarization was never below −55 mV for the NMf-C2. (This may have been offset somewhat by the fact that the NMf-C2 upstroke reached a membrane potential that was between 4 and 14 mV more positive than that of the CM, as discussed by Syed et al. (2005).) Third, the choice of −60 mV as the fixed repolarization threshold eliminated the shortest APDs obtained using the NMf-C2 because the RMP was higher than −60 mV, and the restitution protocol therefore was stopped at a much longer CL than could be reached with our protocol. Finally, the overall restitution protocol differed in that the next AP obtained after only 10 seconds of pacing was used for fitting by Syed et al. (2005), whereas 30 seconds were used in our protocol. As shown in Fig. 5D–E, both the NM and NMf exhibit differences in steady-state APDs obtained after pacing for 5 s and for 30 s, especially for DIs below 400 ms and CLs below 600 ms.

5.2 Relative roles of transmembrane current descriptions and intracellular calcium handling

Exchanging the transmembrane currents formulations of the models elucidates the roles of intracellular calcium handling and ionic currents in these models. Different rate dependencies can be attributed to both. RMP rate dependence is associated with the current formulations of the NM. The rate dependence of APD, on the other hand, is more closely correlated with detailed calcium handling than the transmembrane currents for these models and occurs more strongly for the calcium handling used in the CM. AP morphology when current formulations are exchanged seems more associated with calcium handling than with currents. However, as shown earlier for the CM-N and for the NM-C and NMf-C, other modifications to transmembrane current conductances can also affect AP morphology, so that both current and calcium descriptions appear able to alter this property.

In contrast, memory properties, including the magnitude of differences in S1–S2 restitution curves at long DIs for varying S1 CLs and the direction of APD differences (prolongation or shortening) for various DI values as a function of changes in S1 CL, correlate closely with the transmembrane current formulations, so that calcium handling appears to play only a secondary role in memory properties for these models.

The implications of these findings for modeling are significant. Although transmembrane current formulations appear to be key for RMP rate dependence and for memory properties, intracellular calcium handling is a key determinant of APD rate dependence for these models. However, calcium handling formulations for many models are often based closely on the formulations of other models, with few changes made even when modeling different species or regions of the heart. The differing descriptions of calcium handling have significant consequences for these two models, and it seems likely that calcium dynamics could be equally important in other models. If so, measuring and modeling transmembrane currents relevant to the model will not be sufficient, and intracellular calcium processes will need to be specified more carefully to ensure that APD rate dependence and other properties can be modeled accurately.

Acknowledgements

We gratefully acknowledge support from The Edmond de Rothschild Foundation and from the Heart Science Research Foundation. This research was supported in part by National Heart, Lung, and Blood Institute Grants 5F32HL73604-2 and 1 R15 HL072816-01, and by National Science Foundation Grants MRI-0320865 and PHY05-051164. The computations were performed in part on the National Science Foundation Terascale Computing System at the Pittsburgh Supercomputing Center. We acknowledge the Aspen Center for Physics for support. We also thank F.H. Fenton, A. Nygren, and E.G. Vigmond for useful discussions.

References

Bers DM. Calcium and cardiac rhythms: Physiological and pathophysiological. Circulation Research 2002;90:14–17. [PubMed: 11786512]

Bosch RF, Zeng X, Grammer JB, Popovic K, Mewis C, Kühlkamp V. Ionic mechanisms of electrical remodeling in human atrial fibrillation. Cardiovascular Research 1999;44:121–131. [PubMed: 10615396]

Boutjdir M, Le Heuzey JY, Lavergne T, Chauvaud S, Guize L, Carpentier A, Peronneau P. Inhomogeneity of cellular refractoriness in human atrium: Factor of arrhythmia? Pacing and Clinical Electrophysiology 1986;9(Part II):1095–1100. [PubMed: 2432515]

Brandt MC, Priebe L, Böhle T, Südkamp M, Beuckelmann DJ. The ultrarapid and the transient outward K+ current in human atrial fibrillation. Their possible role in postoperative atrial fibrillation. Journal of Molecular and Cell Cardiology 2000;32:1885–1896.

Cherry EM, Fenton FH. A tale of two dogs: analyzing two models of canine ventricular electrophysiology. American Journal of Physiology 2007;292:H43–H55. [PubMed: 16997886]

Courtemanche M, Ramirez RJ, Nattel S. Ionic mechanisms underlying human atrial action potential properties: insights from a mathematical model. American Journal of Physiology 1998;275:H301–H321. [PubMed: 9688927]

Courtemanche M, Ramirez RJ, Nattel S. Ionic targets for drug therapy and atrial fibrillation-induced electrical remodeling: insights from a mathematical model. Cardiovascular Research 1999;42:477–489. [PubMed: 10533583]

Dobrev D, Ravens U. Remodeling of cardiomyocyte ion channels in human atrial fibrillation. Basic Research in Cardiology 2003;98:137–148. [PubMed: 12883831]

Feng J, Yue L, Wang Z, Nattel S. Ionic mechanisms of regional action potential heterogeneity in the canine right atrium. Circulation Research 1998;83:541–551. [PubMed: 9734477]

Franz MR, Karasik PL, Li C, Moubarak J, Chavez M. Electrical remodeling of the human atrium: Similar effects in patients with chronic atrial fibrillation and atrial flutter. Journal of the American College Cardiology 1997;30:1785–1792.

Grammer JB, Bosch RF, Kühlkamp V, Seipel L. Molecular remodeling of Kv4.3 potassium channels in human atrial fibrillation. Journal of Cardiovascular Electrophysiology 2000;11:626–633. [PubMed: 10868735]

Hund TJ, Kucera JP, Otani NF, Rudy Y. Ionic charge conservation and long-term steady state in the Luo-Rudy dynamic cell model. Biophysical Journal 2001;81:3324–3331. [PubMed: 11720995]

Jeck CD, Boyden PA. Age-related appearance of outward currents may contribute to developmental differences in ventricular repolarization. Circulation Research 1992;71:1390–1403. [PubMed: 1423935]

Kamalvand K, Tan K, Lloyd G, Gill J, Bucknall C, Sulke N. Alterations in atrial electrophysiology associated with chronic atrial fibrillation in man. European Heart Journal 1999;20:888–895. [PubMed: 10329094]

Kim BS, Kim YH, Hwang GS, Pak HN, Lee SC, Shim WJ, Oh DJ, Ro YM. Journal of the American College of Cardiology 2002;39:1329–1336. [PubMed: 11955851]

Koller ML, Riccio ML, Gimour RF Jr. Dynamic restitution of action potential duration during electrical alternans and ventricular fibrillation. American Journal of Physiology 1999;275:H1635–H1642. [PubMed: 9815071]

Li D, Fareh S, Leung TK, Nattel S. Promotion of atrial fibrillation by heart failure in dogs: atrial remodeling of a different sort. Circulation 1999;100:87–95. [PubMed: 10393686]

Lindblad DS, Murphey CR, Clark JW, Giles WR. A model of the action potential and underlying membrane currents in a rabbit atrial cell. American Journal of Physiology 1996;271:H1666–H1691. [PubMed: 8897964]

Luo C, Rudy Y. A dynamic model of the cardiac ventricular action potential. Circulation Research 1994;74:1071–1096. [PubMed: 7514509]

Manios EG, Kanoupakis EM, Chlouverakis GI, Kaleboubas MD, Mavrakis HE, Vardas PE. Changes in atrial electrical properties following cardioversion of chronic atrial fibrillation: relation with recurrence. Cardiovascular Research 2000;47:244–253. [PubMed: 10946061]

Nygren A, Fiset C, Firek L, Clark JW, Lindblad DS, Clark RB, Giles WR. Mathematical model of an adult human atrial cell: the role of K+ currents in repolarization. Circulation Research 1998;82:63–81. [PubMed: 9440706]

Nygren A, Leon LJ, Giles WR. Simulations of the human atrial action potential. Philosophical Transactions of the Royal Society of London A 2001;359:1111–1125.

Osaka T, Itoh A, Kodama I. Action potential remodeling in the human right atrium with chronic lone atrial fibrillation. Pacing and Clinical Electrophysiology 2000;23:960–965. [PubMed: 10879379]

Ramirez RJ, Nattel S, Courtemanche M. Mathematical analysis of canine atrial action potentials: Rate, regional factors, and electrical remodelling. American Journal of Physiology 2000;279:H1767–H1785. [PubMed: 11009464]

Rush S, Larsen H. A practical algorithm for solving dynamic membrane equations. IEEE Transactions on Biomedical Engineering 1978;25:389–392. [PubMed: 689699]

Schotten U, Neuberger HR, Allessie MA. The role of atrial dilatation in the domestication of atrial fibrillation. Progress in Biophysics and Molecular Biology 2003;82:151–162. [PubMed: 12732275]

Schram G, Pourrier M, Melnyk P, Nattel S. Differential distribution of cardiac ion channel expression as a basis for regional specialization in electrical function. Circulation Research 2002;90:939–950. [PubMed: 12016259]

Skasa M, Jüngling E, Picht E, Schöndube F, Lückhoff A. L-type calcium currents in atrial myocytes from patients with persistent and non-persistent atrial fibrillation. Basic Research in Cardiology 2001;96:151–159. [PubMed: 11327333]

Syed Z, Vigmond E, Nattel S, Leon LJ. Atrial cell action potential parameter fitting using genetic algorithms. Medical and Biological Engineering and Computing 2005;43:561–571. [PubMed: 16411628]

Tanabe S, Hata T, Hiraoka M. Effects of estrogen on action potential and membrane currents in guinea pig ventricular myocytes. American Journal of Physiology 1999;277:H826–H833. [PubMed: 10444511]

Van Wagoner DR, Pond AL, McCarthy PM, Trimmer JS, Nerbonne JM. Outward K^+ current densities and Kv1.5 expression are reduced in chronic human atrial fibrillation. Circulation Research 1997;80:772–781. [PubMed: 9168779]

Van Wagoner DR, Pond AL, Lamorgese M, Rossie SS, McCarthy PM, Nerbonne J. Atrial L-type Ca^{2+} currents and human atrial fibrillation. Circulation Research 1999;85:428–436. [PubMed: 10473672]

Victorri B, Vinet A, Roberge FA, Drouhard JP. Numerical integration in the reconstruction of cardiac action potentials using Hodgkin-Huxley-type models. Computers in Biomedical Research 1985;18:10–23.

Workman AJ, Kane KA, Rankin AC. The contribution of ionic currents to changes in refractoriness of human atrial myocytes associated with chronic atrial fibrillation. Cardiovascular Research 2001;52:226–235. [PubMed: 11684070]

Xiao L, Zhang L, Han W, Wang Z, Nattel S. Sex-based transmural differences in cardiac repolarization and ionic-current properties in canine left ventricles. American Journal of Physiology 2006;291:H570–H580. [PubMed: 16501015]

Xie F, Qu Z, Garfinkel A, Weiss JN. Electrical refractory period restitution and spiral wave reentry in simulated cardiac tissue. American Journal of Physiology 2002;283:H448–H460. [PubMed: 12063320]

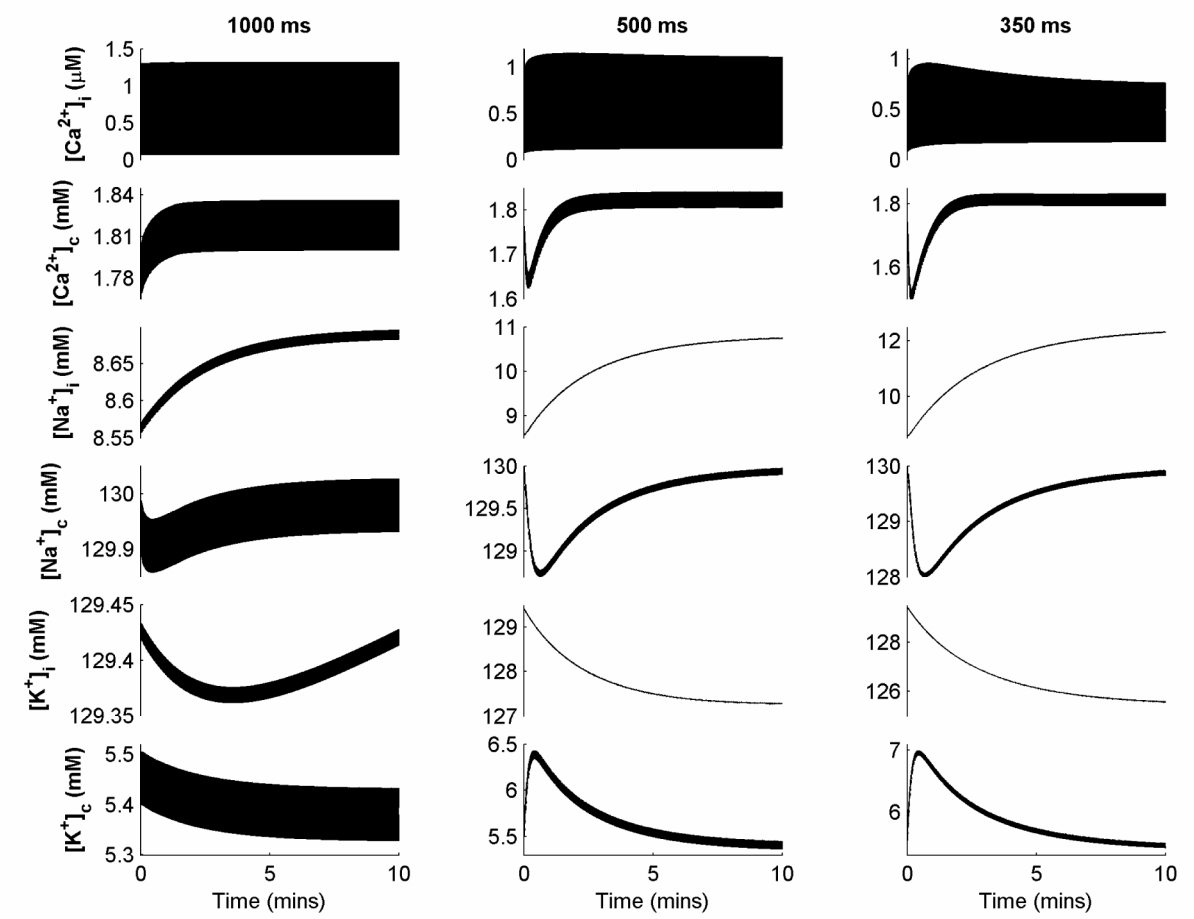

Figure 1.

Variations in ionic concentrations over 10 minutes of constant pacing at cycle lengths (CLs) of 1000, 500, and 350 ms for the NM. Note that different scales are used for each concentration and each CL to indicate ongoing adjustments to concentrations appropriately.

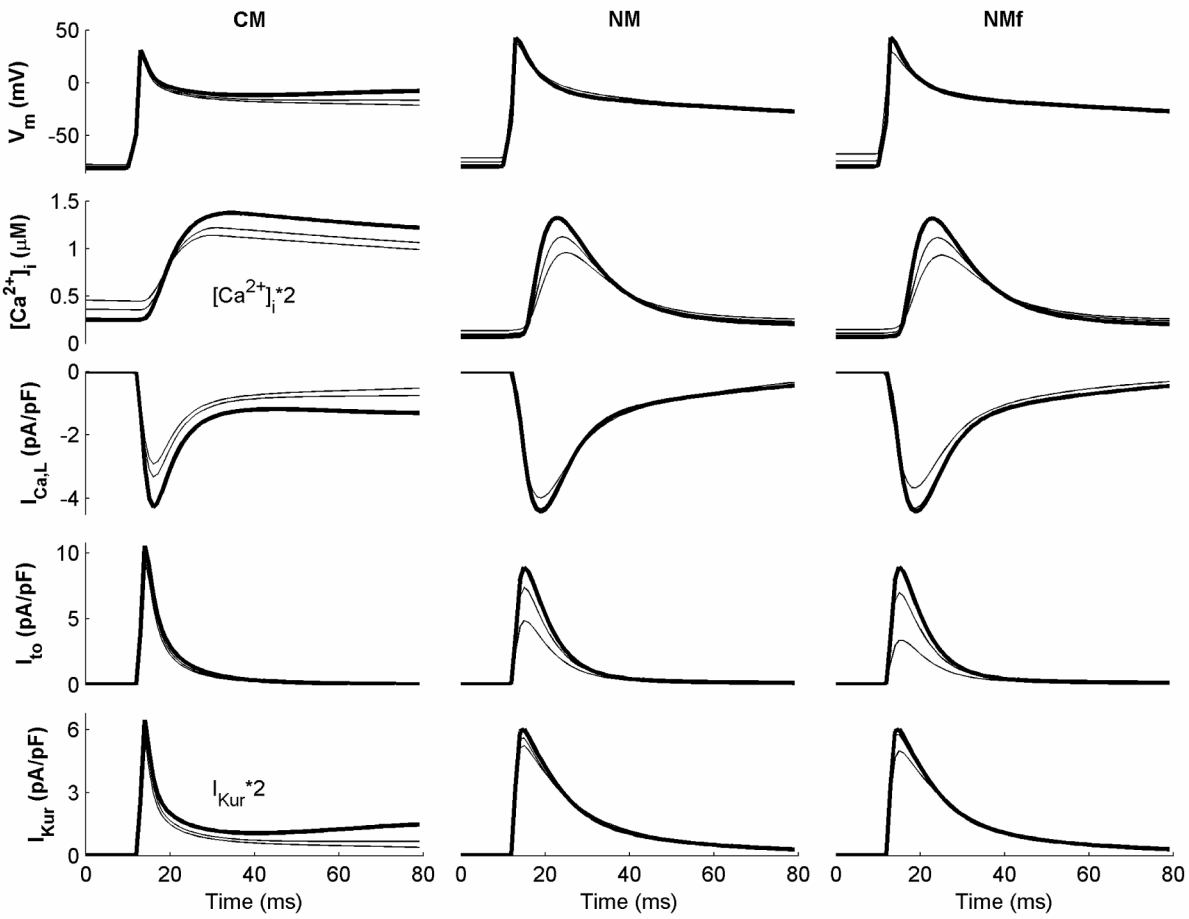

Figure 2.

Important transmembrane currents and the calcium transient $[Ca^{2+}]_i$ during the first 80 ms of an action potential (AP) for the CM, NM, and NMf at CLs of 1000, 500, and 350 ms. All currents are shown for the last action potential (AP) obtained during 30 seconds of pacing at the given CL. Currents at a CL of 1000 ms are shown in bold. Note that some traces have been rescaled as indicated.

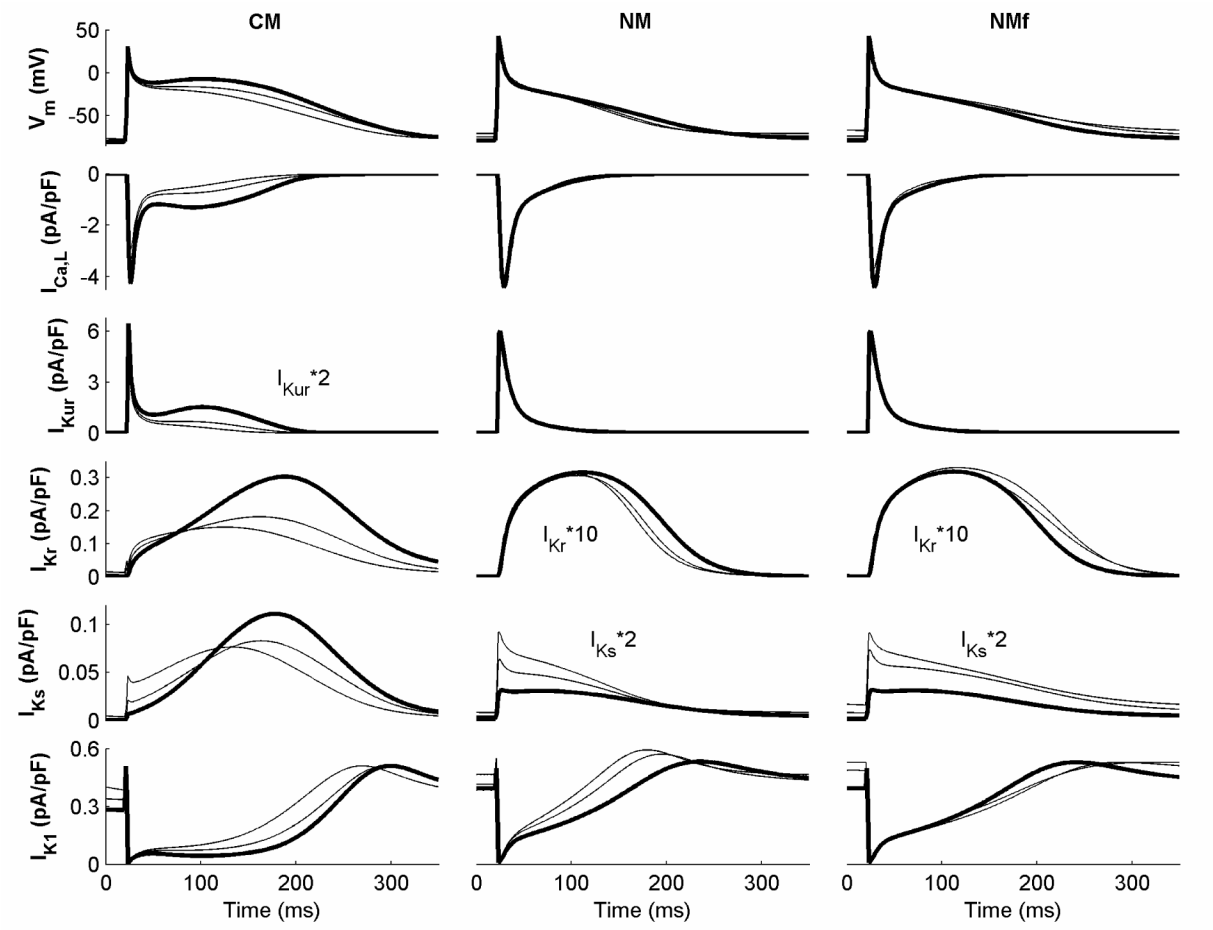

Figure 3.

Important transmembrane currents during the first 350 ms of an AP for the CM, NM, and NMf at CLs of 1000, 500, and 350 ms. All currents are shown for the last AP obtained during 30 seconds of pacing at the given CL. Currents at a CL of 1000 ms are shown in bold. Note that some traces have been rescaled as indicated.

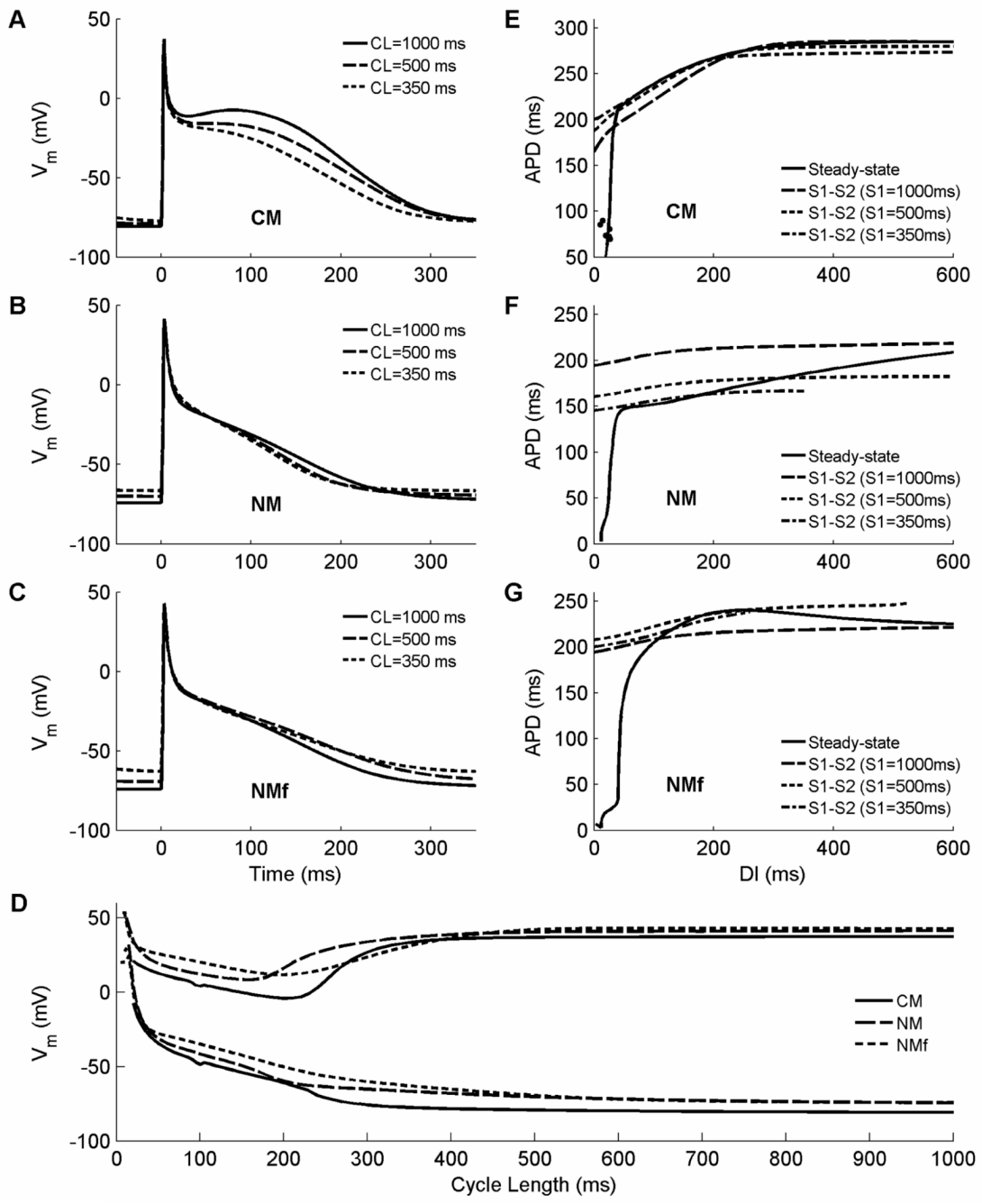

Figure 4.

A–C. Rate dependence of AP morphology and duration at CLs of 1000 ms (solid), 500 ms (dashed), and 350 ms (dotted) for (A) the CM, (B) the NM, and (C) the NMf. Each AP is the last in a 30-second interval of pacing at the specified CL. Only the CM exhibits significant rate dependence of AP duration (APD) and shape, switching from spike-and-dome morphology at long CLs to triangular morphology at short CLs, whereas the NM and NM-f exhibit significant rate dependence of resting membrane potential (RMP), which increases with decreasing CL. **D**. Resting and peak membrane potentials as a function of CL for the CM (solid), NM (long dashes), and NMf (short dashes). As CL decreases, all of the models show an increase in RMP along with a decrease followed by an increase in peak membrane potential. **E–G**. Restitution

of APD_{90} for (E) the CM, (F) the NM, and (G) the NMf. Steady-state restitution curves (solid lines) obtained after pacing for 30 seconds at each CL are shown along with S1–S2 restitution curves obtained after 30 seconds of pacing at S1 CLs of 1000 ms (long dashes), 500 ms (short dashes), and 350 ms (dash-dots). The CM shows increasing APDs in S1–S2 curves with decreasing S1 CL at short DIs, as does the NMf at long CLs. The NMf also has a slightly biphasic steady-state restitution curve, as does the CM at longer DIs than shown here. Alternans occur only in the CM and are shown using filled circles. Note that although different maximum and minimum values of APD are shown, the scaling is the same for the three panels. Stimulus is twice diastolic threshold and is applied for 3 ms here and throughout.

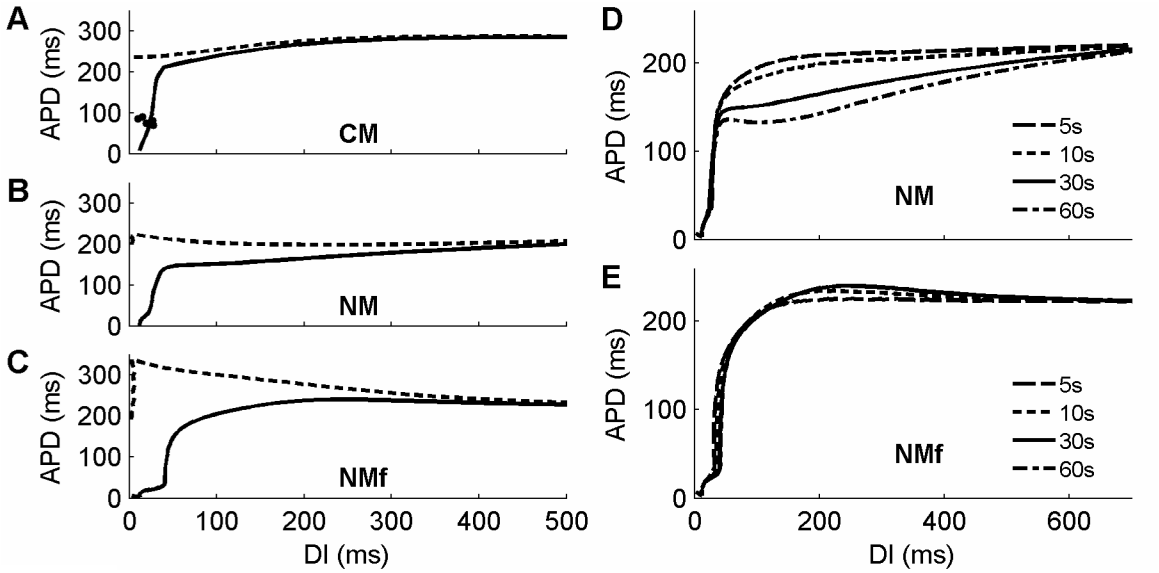

Figure 5.

Issues associated with calculating restitution curves. **A–C**. Calculation of steady-state APD restitution curves using either a non-varying fixed voltage threshold (dashed) or CL-dependent threshold associated with APD_{90} (solid) for (A) the CM, (B) the NM, and (C) the NMf. The differences between the two curves are not substantial at long DIs but become significant at shorter DIs. In addition, the shapes of the curves are modified by using a constant voltage threshold for APD calculation, which makes the curves for the NM and NMf have larger regions of negative slope when not using CL-dependent APD_{90}. Alternans in the CM are shown using filled circles. **D–E**. Calculation of steady-state APD restitution curves using the NM. When ionic concentrations vary freely (D), drift in these concentrations does not allow the model to reach steady-state even after 60 seconds of pacing. Consequently, action potentials for a given CL continually decrease over time, and a steady-state restitution curve cannot be obtained, even after several minutes (see Figure 1). When ionic concentrations are fixed in the NMf (E), steady-state is reached within 30 seconds of pacing, and little variation is seen with only 10 seconds of pacing.

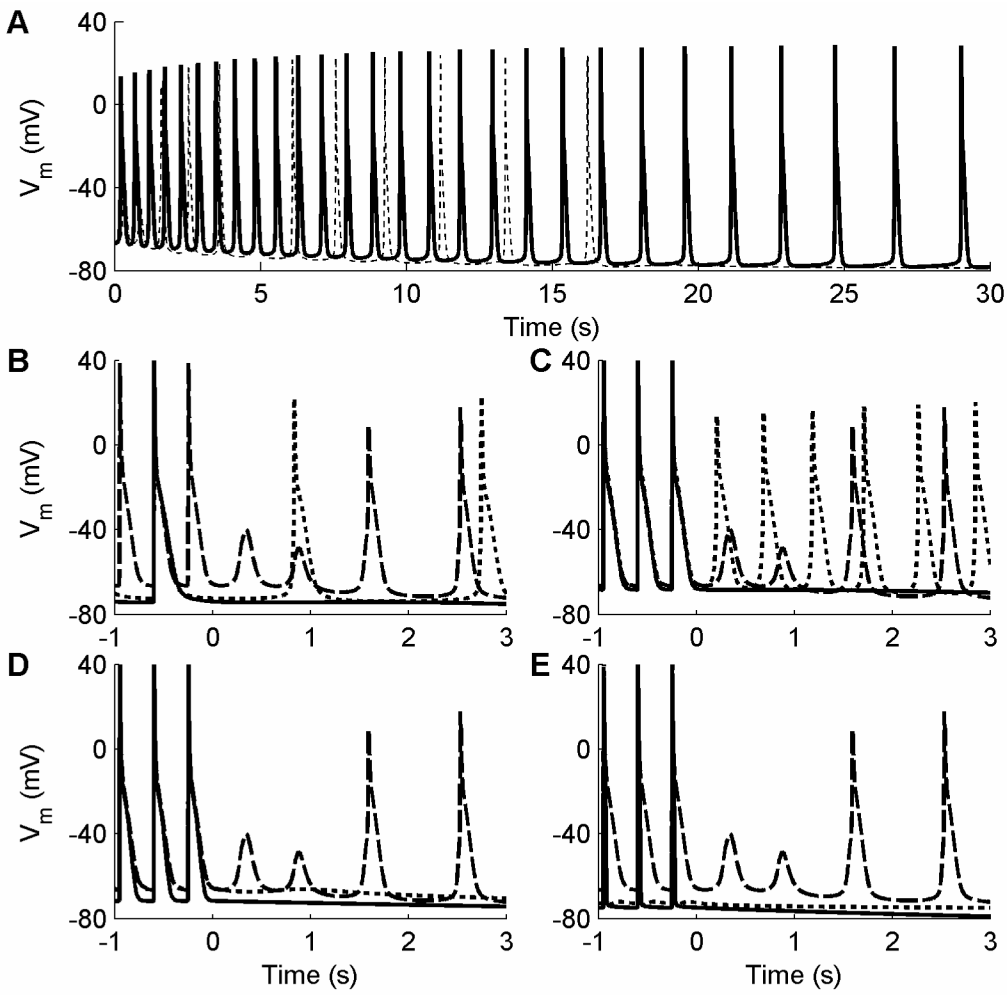

Figure 6.

Delayed afterdepolarizations (DADs) and auto-oscillatory behavior in the NM induced after pacing for 30 s at a given CL and then ceasing pacing (at time = 0). **A**. DADs induced after pacing at a CL of 350 ms under normal conditions (dotted) and with the buffering variable O_{TMgMg} held constant (solid). Under normal conditions, the afterdepolarization activity died out within 17 s. In both cases, the DAD frequency decreased over time. **B**. Activity induced under normal conditions after pacing at CLs of 350 ms (dashed), 700 ms (dotted), and 1050 ms (solid). DADs are suppressed entirely at the 1050 ms CL and are spaced farther apart in time for 700 ms than for 350 ms. **C**. Activity induced after pacing at a CL of 350 ms under normal conditions (dashed), with O_{TMgMg} held constant (dotted), and with the buffering variable O_{TC} held constant (solid). **D**. Activity induced after pacing at a CL of 350 ms under normal conditions (dashed), with the time rate of change of the buffer occupancy dO/dt multiplied by 4 (dotted), and with I_{NaCa} multiplied by 0.1 (solid). **E**. Activity induced after pacing at a CL of 350 ms under normal conditions (dashed), with with I_{Kr} multiplied by 500 (dotted), and with I_{K1} multiplied by 10 (solid).

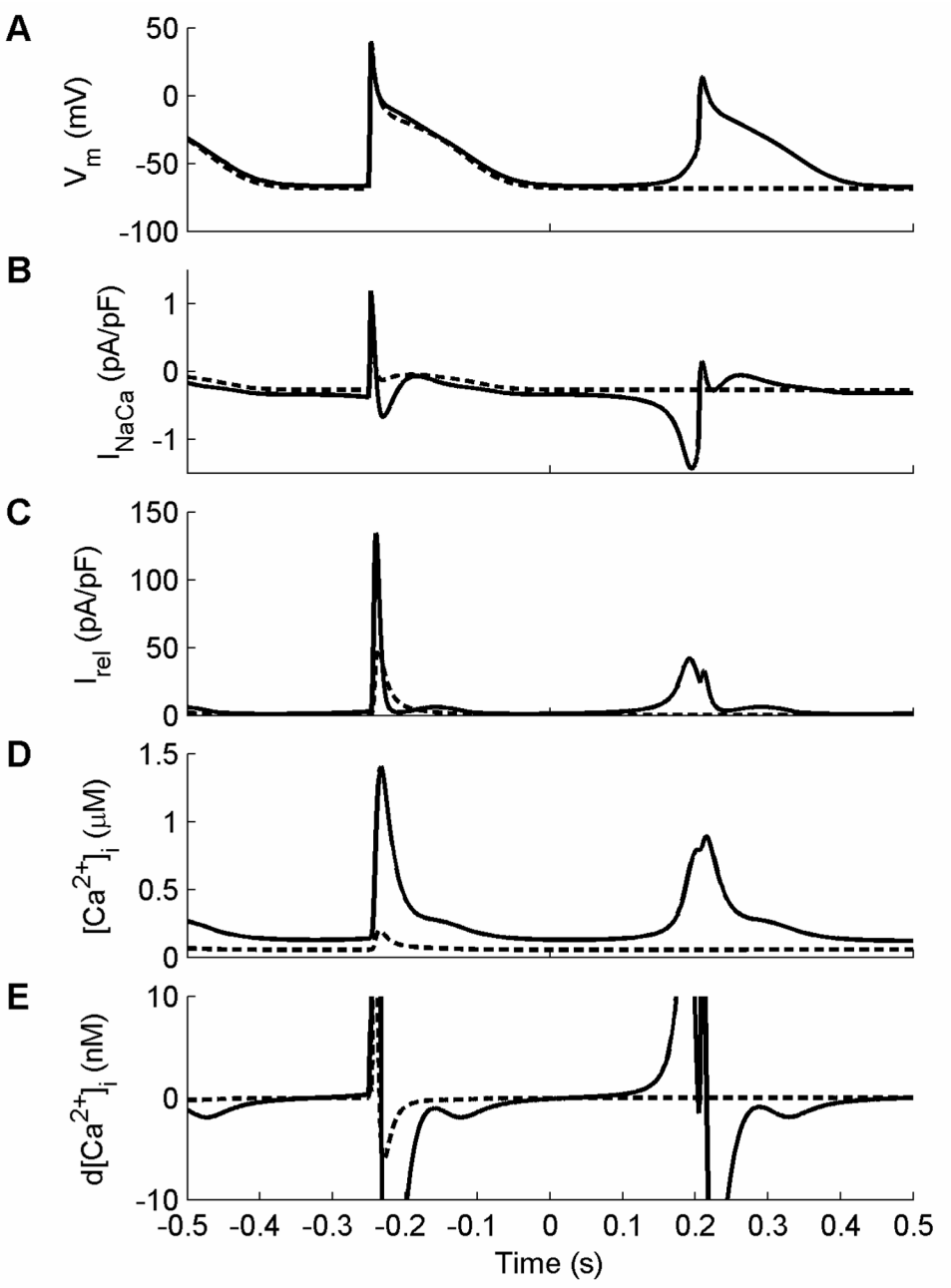

Figure 7.

Dynamics of DADs in the NM with O_{TMgMg} clamped and with the buffering variable O_C clamped (dashed). Pacing was maintained at a CL of 350 ms for 30 s, after which pacing was discontinued (time = 0). **A**. Voltage behavior for the two cases: clamping O_C prevents DADs following cessation of pacing. **B**. The initial depolarization when O_{TMgMg} is held constant is due to I_{NaCa}, which responds to an increase in $[Ca^{2+}]_i$ by increasing in magnitude. The upstroke of the DAD-induced AP therefore is slow early on, when it is controlled by I_{NaCa}, and then more rapid as the voltage reaches the threshold for I_{Na} activation. When O_C is held constant instead, I_{NaCa} does not depolarize the cell. **C**. Early calcium release from the SR occurs when O_{TMgMg} is clamped but not when O_C is clamped. The release current in this case is of a smaller magnitude but for a longer time and begins well before the AP upstroke. **D**. The gradual

depolarization following the last paced beat when O_{TMgMg} is clamped coincides with a slow increase in $[Ca^{2+}]_i$, which leads to the increase in the magnitude of I_{NaCa}. The calcium transient is much smaller when O_C is clamped instead, and it does not increase following cessation of pacing. **E**. The initial increase in $[Ca^{2+}]_i$ following cessation of pacing when O_{TMgMg} is clamped occurs when the sign of $d[Ca^{2+}]_i$ changes from negative to positive; here the plotted range of $d[Ca^{2+}]_i$ has been reduced to illustrate this occurrence. When O_C is clamped instead, no sign change occurs until the beginning of the upstroke of a paced beat. The sign of $d[Ca^{2+}]_i$ depends directly on the balance of three transmembrane currents, three intracellular calcium currents, and the rate of change of three calcium buffering variables, as well as indirectly on a number of other variables, all of which allows for numerous possibilities for enhancing or suppressing DADs.

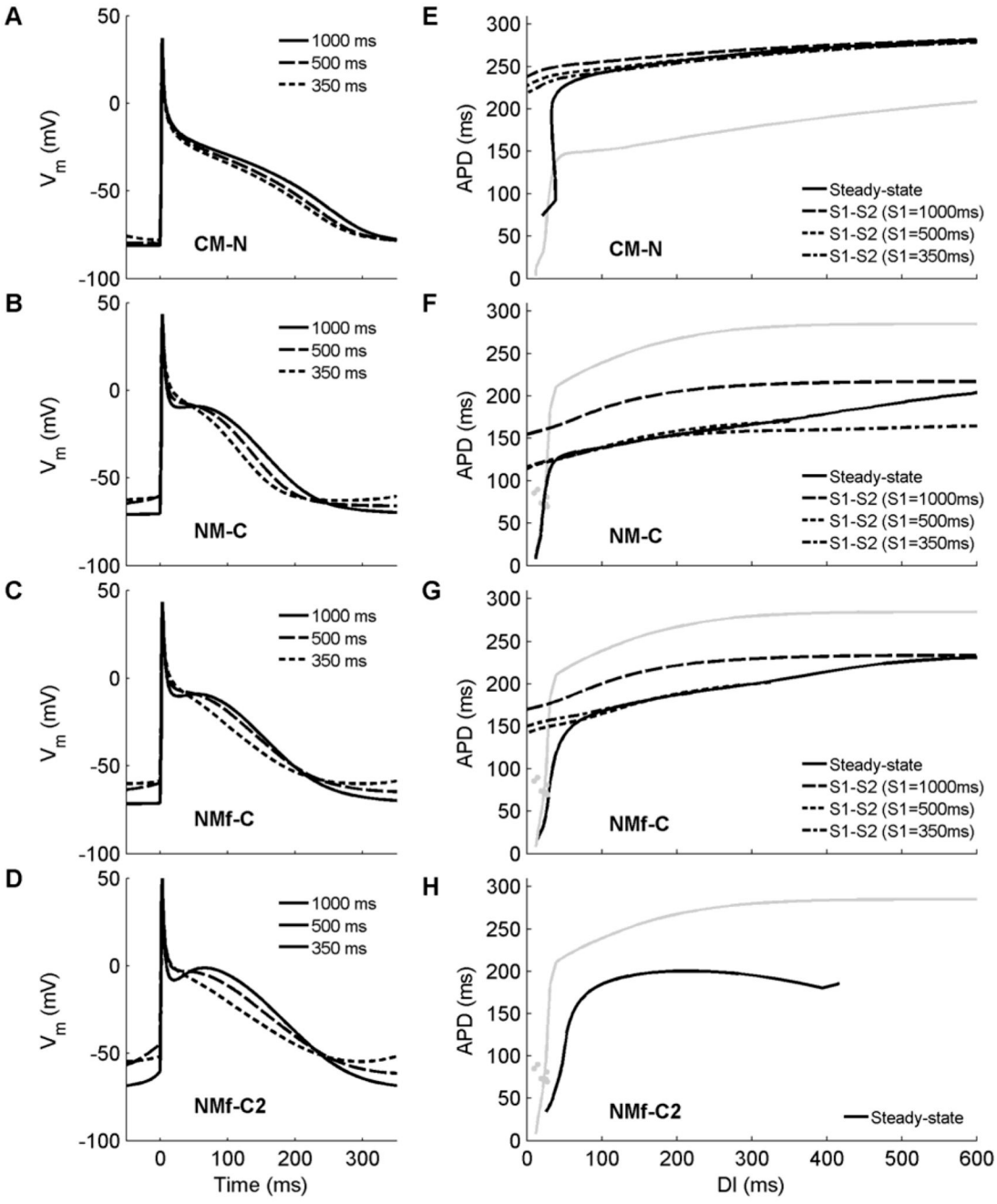

Figure 8.

Action potentials and restitution curves obtained using modifications to current magnitudes suggested to improve agreement between the two models, as proposed by Nygren et al. (2001) and Syed et al. (2005). **A–D**. Action potentials after 30 seconds of pacing at CLs of 1000, 500, and 350 ms for (A) the CM-N, (B) the NM-C, (C) the NMf-C, and (D) the NMf-C2; compare with Figure 4A–C. Although the modifications have some effects on the overall APs, the rate dependence of APD, AP morphology, and RMP are different compared to the original NM and CM the model variants seek to reproduce. **E–H**. Restitution of APD_{90} for (E) the CM-N, (F) the NM-C, (G) the NMf-C, and (H) the NMf-C2; compare with Figure 4E–G. Steady-state restitution curves (solid lines) obtained after pacing for 30 seconds at each CL are

shown along with S1–S2 restitution curves obtained after 30 seconds of pacing at S1 CLs of 1000 ms (long dashes), 500 ms (short dashes), and 350 ms (dash-dots). Gray lines indicate the steady-state restitution curve of the model each variant seeks to emulate (the NM for E, and the CM for F–H). Applying the inverse of the proposed changes to the original CM (D) eliminates nearly all memory from the system; restitution curves obtained using steady-state and S1–S2 protocols are nearly identical, with almost no dependence on S1 CL. However, the restitution curve still differs from the restitution curves of the NM and NMf, and instead is similar to the steady-state restitution curve obtained without modifications. Using the proposed modifications to the original NM (F) minimally affects the restitutions curves; APDs and the minimum DI are slightly decreased. However, decreasing the S1 CL results in shorter APDs, unlike the original CM, where longer APDs occur. Furthermore, all APDs, especially the smallest APDs during steady–state pacing, are significantly shorter than for the original CM. Application of the proposed modifications to the NMf (G) eliminates the biphasic portion of the restitution curve and steepens the curve overall. However, the S1-dependence of the S1–S2 protocols remains inverted to that of the original CM, and APDs overall remain shorter. For the NMf-C2, S1-S2 restitution curves cannot be obtained for all S1 CLs over all diastolic intervals for the NMf-C2 due to pronounced DADs. For the steady-state curve, APD_{90} remains longer for the CM than for the NMf-C2.

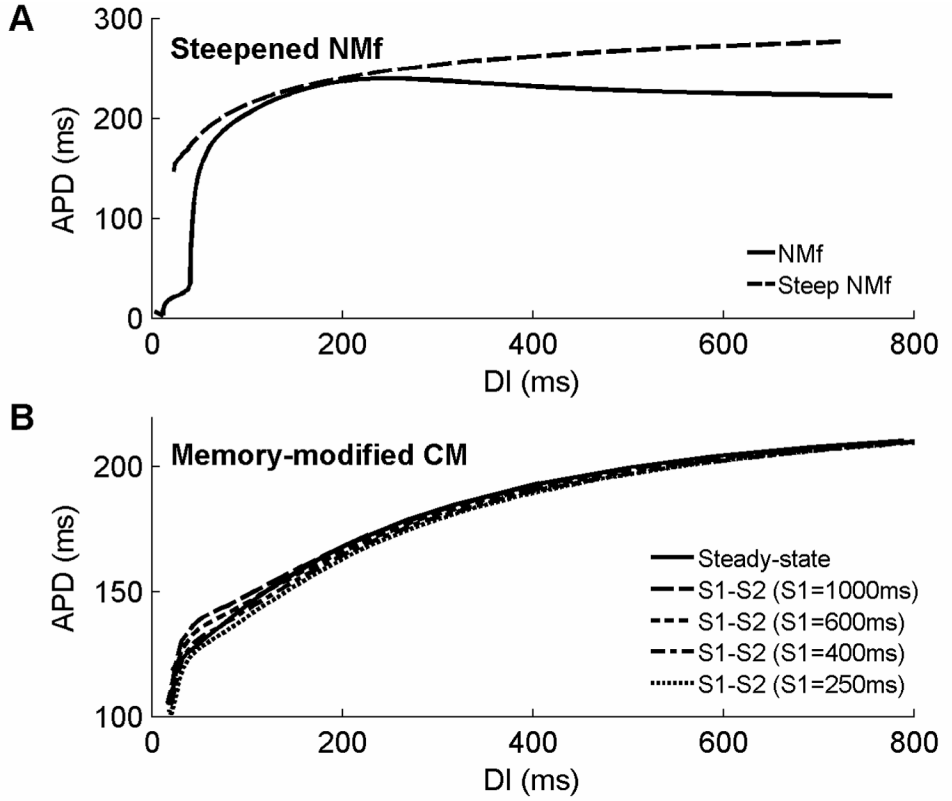

Figure 9.

Modified restitution curves for the original CM and the NMf. **A**. Modifications to currents in the original NMf can produce a steeper steady-state restitution curve over a broader range of DIs. In addition, these modifications remove the extremely short APDs at extremely short DIs and eliminate the biphasic region of the steady-state restitution curve. Although the restitution curve is steepened, its slope is only greater than one for DIs smaller than 45ms. See text for details. **B**. Modifications to currents in the original CM can reverse the dependence of S1–S2 restitution curves on S1 CL at short DIs. In the present arrangement, APDs decrease with decreasing S1 CL as well as with decreasing DI.

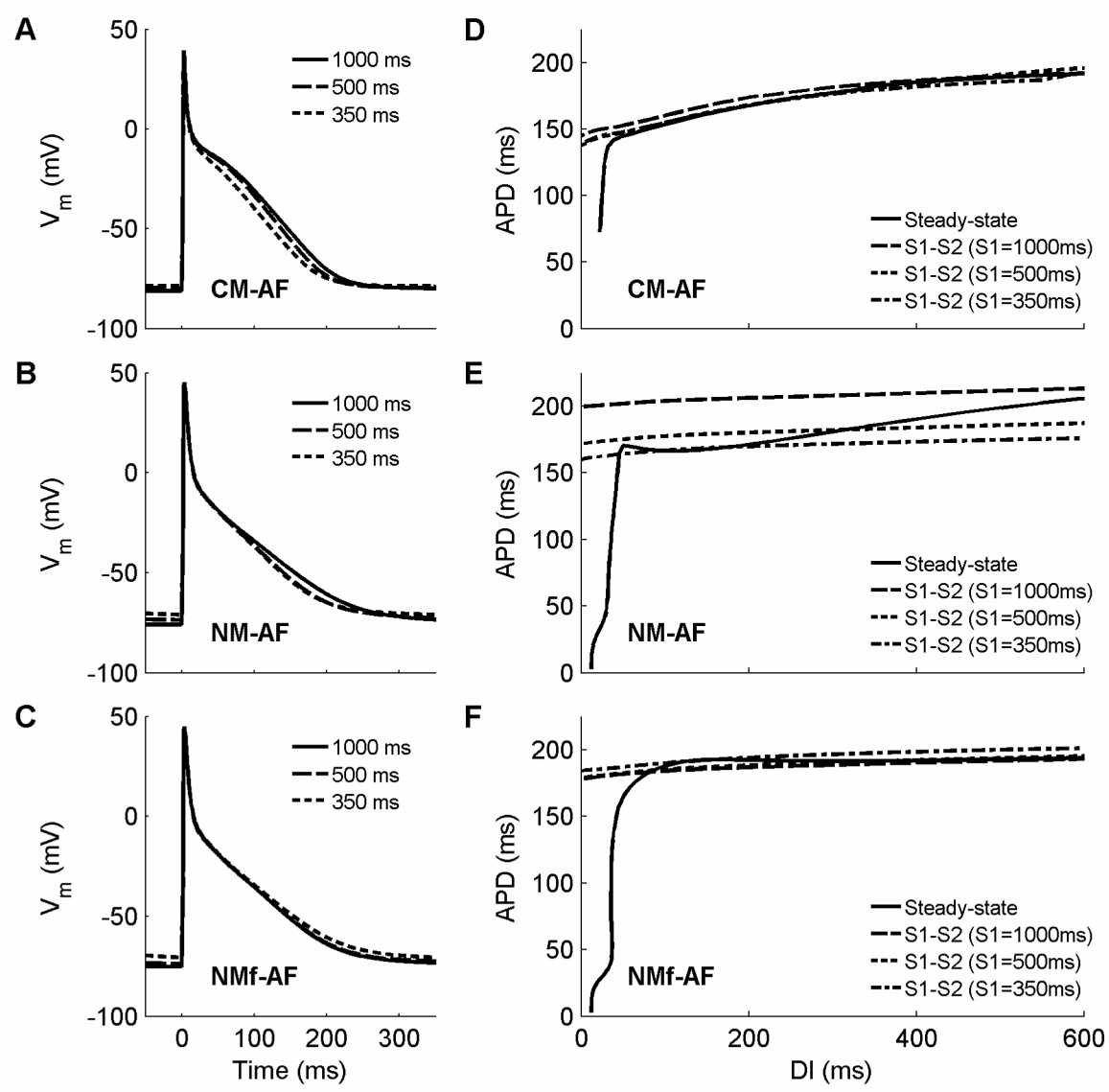

Figure 10.

Action potentials and restitution curves after 30 seconds of pacing using the current magnitude modifications of Courtemanche et al. (1999) to simulate AF-induced electrophysiological changes. **A–C**. Action potentials at CLs of 1000, 500, and 350 ms are shown for (A) the CM-AF, (B) the NM-AF, and (C) the NMf-AF. Agreement among the models is substantially greater under these conditions, although the RMPs in the CM-AF generally remain lower than in the NM-AF and NMf-AF. **D–F**. Restitution of APD_{90} for (D) the CM-AF, (E) the NM-AF, and (F) the NMf-AF. Steady-state restitution curves (solid lines) obtained after pacing for 30 seconds at each CL are shown along with S1–S2 restitution curves obtained after 30 seconds of pacing at S1 CLs of 1000 ms (long dashes), 500 ms (short dashes), and 350 ms (dash-dots). The restitution curves obtained using steady-state and S1–S2 protocols for the CM-AF, like those for the CM-N, are nearly identical, indicating that nearly all memory has been eliminated. The modifications hardly affect the original NM's restitution; if anything, action potentials are slightly prolonged for the NM-AF. For the NMf-AF, the APDs are decreased slightly, but the overall shapes of the curves remain quite similar to those obtained without modifications.

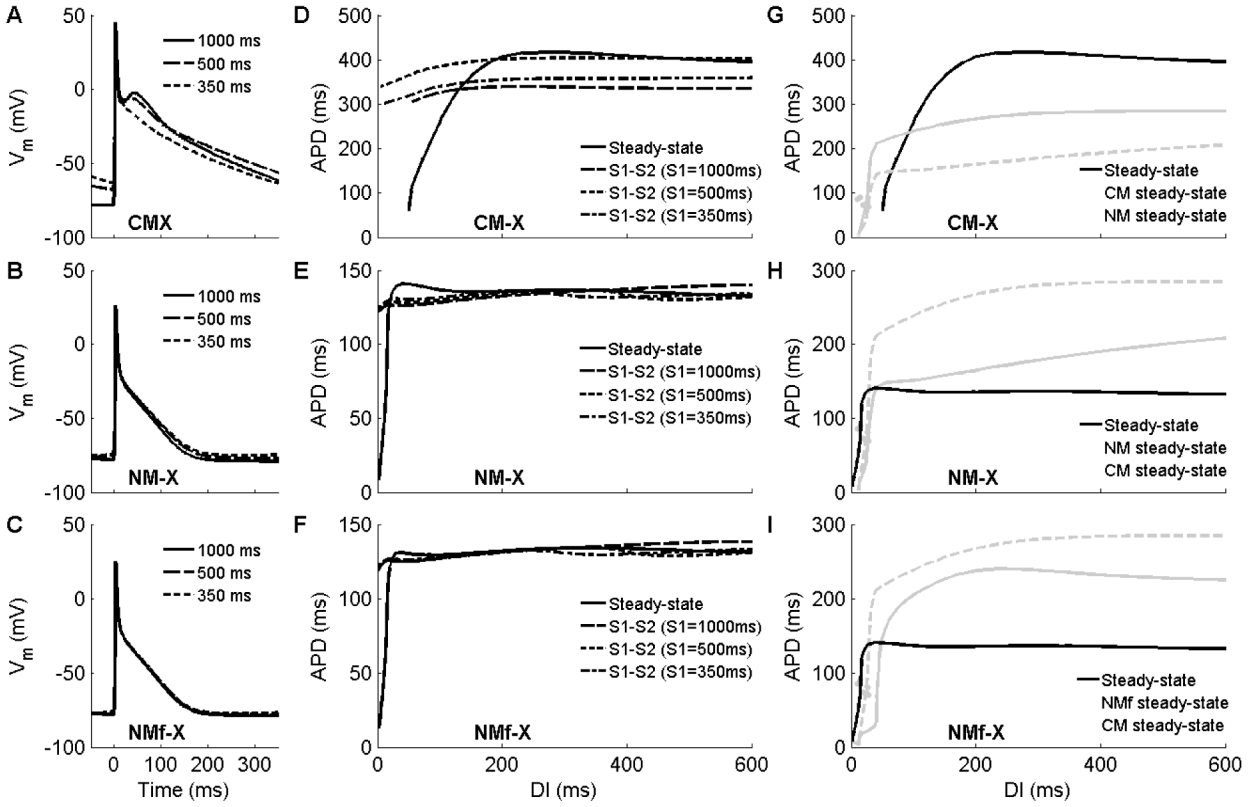

Figure 11.

Action potentials and restitution curves obtained by interchanging the 12 transmembrane current formulations used by the models. **A–C**. Action potentials after 30 seconds of pacing at CLs of 1000, 500, and 350 ms for (A) the CM-X, (B) the NM-X, and (C) the NMf-X. Although the rate dependence of RMP follows the transmembrane current descriptions, the rate dependence of APD and AP morphology appear to be determined primarily by calcium handling. **D–F**. Restitution of APD_{90} for (D) the CM-X, (E) the NM-X, and (F) the NMf-X. Steady-state restitution properties including curve flatness and biphasic segments appear to be determined by calcium handling and other ionic concentrations, while the memory properties as evidenced by S1–S2 restitution curves appear more closely tied to the transmembrane current descriptions. Note that the plot scales are varied. G–I. Steady-state restitution of APD_{90} for (G) the CM-X, (H) the NM-X, and (I) the NMf-X, plotted together with steady-state restitution curves of the NM and CM. Note that the plot scales are varied.

Table 1

Abbreviations and descriptions of the model variants used.

Abbreviation	Model Variant Description
NM	Nygren et al. model
NMf	Nygren et al. model with the following concentrations held constant: $[K^+]_i$, $[K^+]_c$, $[Na^+]_i$, $[Na^+]_c$, $[Ca^{2+}]_c$
NM-C	Nygren et al. model with $I_{Ca,L}$ multiplied by 1.33, I_{to} by 2, I_{Kur} by 0.4, I_{Kr} by 3, and I_{Ks} by 3 (from Nygren et al., 2001)
NMf-C	Nygren et al. model with $I_{Ca,L}$ multiplied by 1.33, I_{to} by 2, I_{Kur} by 0.4, I_{Kr} by 3, and I_{Ks} by 3 (from Nygren et al., 2001) and with the following concentrations held constant: $[K^+]_i$, $[K^+]_c$, $[Na^+]_I$, $[Na^+]_c$, $[Ca^{2+}]_c$
NMf-C2	Nygren et al. model with I_{Na} multiplied by 0.938, $I_{Ca,L}$ by 1.37, I_{to} by 2.07, I_{Kur} by 0.196, I_{Ks} by 1.50, I_{Kr} by 1.56, I_{K1} by 1.07, I_{Nab} by 1.02, and I_{Cab} by 1.02 (from Syed et al., 2005) and with the following concentrations held constant: $[K^+]_i$, $[K^+]_c$, $[Na^+]_i$, $[Na^+]_c$, $[Ca^{2+}]_c$
NM-AF	Nygren et al. model with $I_{Ca,L}$ multiplied by 0.3, I_{to} by 0.5, and I_{Kur} by 0.5 (from Courtemanche et al., 1999)
NMf-AF	Nygren et al. model with $I_{Ca,L}$ multiplied by 0.3, I_{to} by 0.5, and I_{Kur} by 0.5 (from Courtemanche et al., 1999) and with the following concentrations held constant: $[K^+]_i$, $[K^+]_c$, $[Na^+]_i$, $[Na^+]_c$, $[Ca^{2+}]_c$
NM-X	Nygren et al. model formulations of ionic concentrations and calcium handling combined with the 12 transmembrane currents of the Courtemanche et al. model
NMf-X	Nygren et al. model formulations of calcium handling combined with the 12 transmembrane currents of the Courtemanche et al. model and with the following concentrations held constant: $[K^+]_i$, $[K^+]_c$, $[Na^+]_i$, $[Na^+]_c$, $[Ca^{2+}]_c$
CM	Courtemanche et al. model with $[K^+]_i$, $[Na^+]_i$ held fixed
CM-N	Courtemanche et al. model with $I_{Ca,L}$ divided by 1.33, I_{to} by 2, I_{Kur} by 0.4, I_{Kr} by 3, and I_{Ks} by 3 (from Nygren et al., 2001) and with $[K^+]_i$, $[Na^+]_i$ held fixed
CM-AF	Courtemanche et al. model with $I_{Ca,L}$ multiplied by 0.3, I_{to} by 0.5, and I_{Kur} by 0.5 (from Courtemanche et al., 1999) and with $[K^+]_i$, $[Na^+]_i$ held fixed
CM-X	Courtemanche et al. model formulations of calcium handling combined with the 12 transmembrane currents of the Nygren et al. model and with $[K^+]_i$, $[Na^+]_i$ held fixed